# Nonisothermal Synthesis of Homogeneous and Multiphase Reactor Networks

**Vipul L. Mehta and Antonis C. Kokossis**
Dept. of Process Integration, UMIST, P.O. Box 88, Manchester, M60 1QD, UK

*A new optimization method for the synthesis of nonisothermal reactor networks offers major challenges concerning the lack of robustness in the existing methods and the numerous local and near-optimal solutions that characterize these problems. The approach offers a reliable and widely tested methodology that upholds a profile-based search. The search concentrates on targets rather than network details. The results illustrate ways to avoid unnecessarily complicated networks and develop simpler and transparent designs. The single-phase examples explain merits over past studies and other conventional synthesis methods. Multiphase examples are presented for the first time in the literature, as well as results from an industrial example.*

## Introduction

The synthesis of nonisothermal reactor networks mostly relates to fixed reactor structures. Nonisothermal cascades of adiabatic beds and stirred-tank reactors have been extensively researched by Aris (1960a,b,c,d, 1961a,b, 1962, 1964) using dynamic programming techniques. Dyson and Horn (1967) optimized the feed distributions of tubular reactors (homogeneous, single-reaction); Dyson et al. (1967) optimized their temperature profiles; and Dyson and Horn (1969) the required amount of catalyst. Chitra and Govind (1985a,b) included intermediate levels of mixing with serial networks of recycled reactors. Achenie and Biegler (1990) optimized recycled reactors with indirect heat-transfer options. Kokossis and Floudas (1990, 1994a,b) proposed a general superstructure of ideal CSTRs and PFRs. They considered all flow and mixing patterns with different feeding, recycling, and bypassing strategies. The PFRs were approximated by cascades of adiabatic sub-PFRs (SPFRs) and featured intermediate heaters, coolers, and intermediate injections of feed. Marcoulaki and Kokossis (1999) recently extended this methodology with the use of stochastic optimization. They enabled its application to highly nonlinear kinetics, but maintained limited emphasis on nonisothermal problems.

In the meantime, Glasser and coworkers (Glasser and Hildebrandt, 1997; Glasser et al., 1987, 1992, 1994; Hildebrandt and Biegler, 1994; Hildebrandt and Glasser, 1990; Hildebrandt et al., 1990; Hopley et al., 1996; Nicole et al., 1997) brought new life into the early ideas of Horn (1964) and his attainable-region concept. They recommend the use of graphical procedures that are particularly insightful for the study of single reactions. The analysis, however, appears less promising for higher dimensions where mathematical optimization techniques become inevitable. Balakrishna and Biegler (1992a,b, 1993) presented an approach that addressed an optimal-control problem and was solved using NLP techniques. Lakshamanan and Biegler (1996) applied MINLP techniques on a serial superstructure of ideal CSTRs, PFRs and DSRs. Schweiger and Floudas (1999) applied optimal-control techniques on similar layouts.

Even in terms of a simulation problem, the nonisothermal reactor represents a rather challenging system. In practice, options are quickly reviewed by comparing the performance of some simple cases (Figure 1) whose design parameters are set fixed to values dictated by experience and intuition. The optimization of the reactor performance introduces numerous, if not infinite, alternatives with a near-optimal performance. The case of the single exothermic reaction is an excellent illustration for this argument: the optimal profile may be unique, but there exists an infinite sequence of adiabatic cascades that can trace the profile. The simultaneous consideration of structural and operational aspects—in the way attempted by comprehensive representations and superstructures—further complicates the picture. The large population of candidates is now introduced both for global and local minima. Furthermore, only few of the available candidates remain simple and transparent enough to explain the trade-

Correspondence concerning this article should be addressed to A. C. Kokossis at this current address: Dept. of Chemical and Process Engineering, School of Engineering in the Environment, Univ. of Surrey, Guildford, GU2 7XH, U.K.
Current address of V. L. Mehta: Bayer AG, ZT-TE 7.1, Process Synthesis Building E41, D-51368, Leverkusen, Germany.

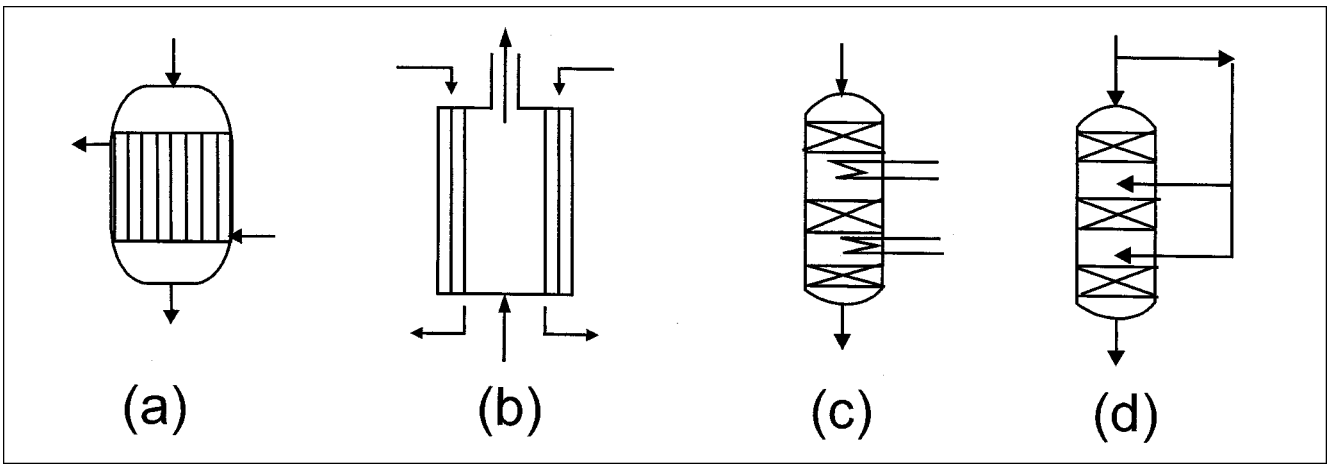


**Figure 1. Heat-transfer options for nonisothermal reactors.**

offs; the large majority of near-optimal candidates assume complicated layouts that carry little information to the designer. A useful synthesis approach should ensure that (1) all the design novelty is contained in the synthesis model; (2) the optimization is robust; and (3) multiplicities are controlled so that the synthesis is not consumed in a wasteful effort. This article outlines an approach that claims merits at all fronts. It presents a method that is applicable to both homogeneous and multiphase systems. Rather than expanding isothermal superstructures with heat-transfer units (Achienie and Biegler, 1988, 1990; Chitra and Govind, 1985b; Kokossis and Floudas, 1994a,b; Marcoulaki and Kokossis, 1999), the article explains the use of temperature profiles and reports benefits over conventional techniques.

## Problem Description

The nonisothermal problem is a misleadingly simple variation of the isothermal case. At least its description reads rather similar.

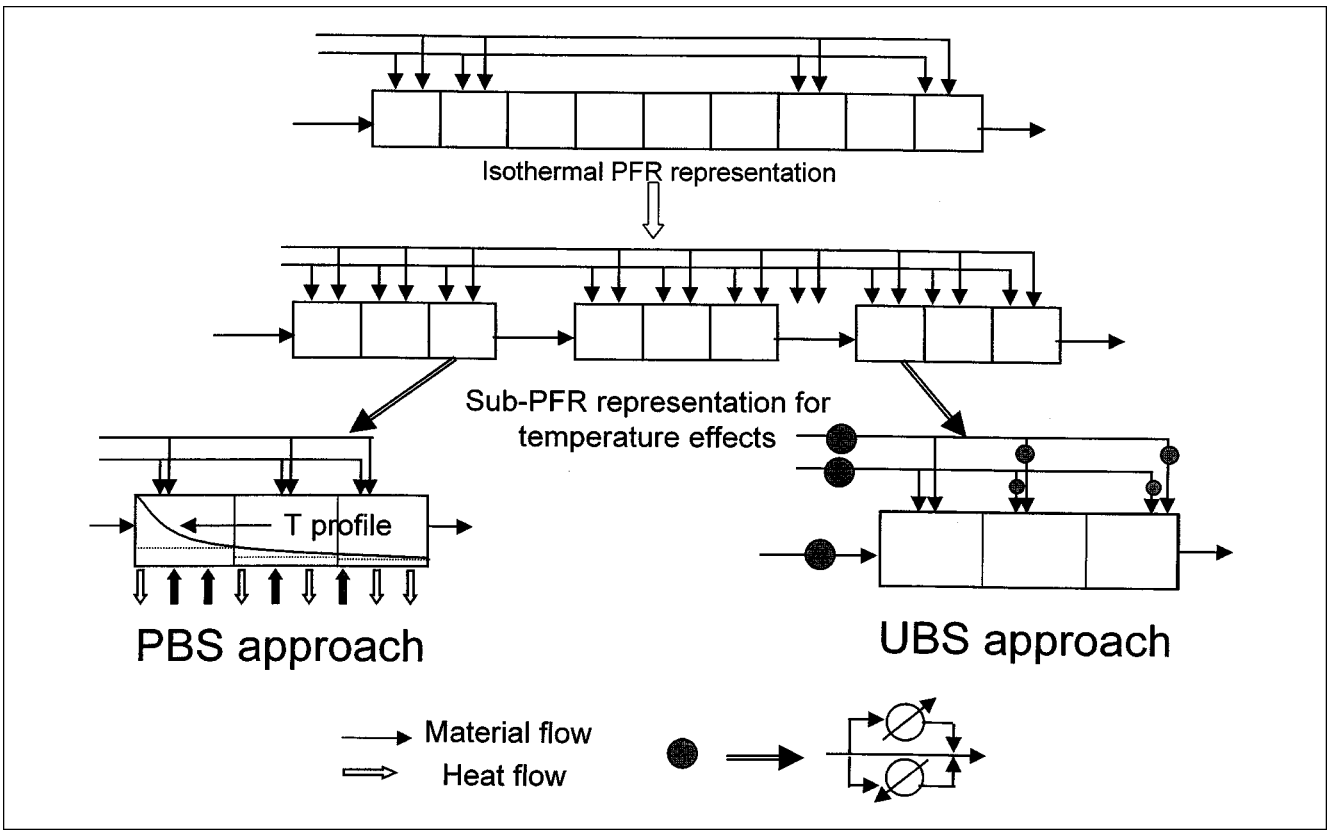


**Figure 2. Nonisothermal representation for an ideal PFR.**

For given (1) reaction mechanism and kinetics; (2) mass-transfer models; (3) phase equilibrium and thermodynamic properties (heat of reaction, evaporation and solubility); and (4) known dependencies on the temperature, the synthesis approach should determine (1) performance targets of the reaction process; (2) layouts of promising solutions; and (3) temperature control policies appropriate to achieve the targets.

Simple extensions of isothermal superstructures (with additional heat-transfer units and energy balances) entail fundamental limitations. Unable to control the layout complexity, they introduce a large, if not infinite, number of similar solutions that deprive the optimization from its robustness. The optimization is much easier for a known temperature profile: once the optimal profile is determined, layouts can be developed easily. This basic observation leads to a two-stage synthesis effort that optimizes the development of the:

1. Temperature profiles that maximize the performance, and

2. Continues with the reactor network development appropriate to produce the selected profile.

The *profile-based synthesis* stage (PBS) is a targeting stage. Layout details and the selection of the heat-transfer units are left for a subsequent level. The PBS is compared with a conventional *unit-based-synthesis* (UBS) approach where temperatures and heat-exchanger units (coolers, heaters) are optimized simultaneously. This article presents applications of single and multiphase systems. It assumes thermal equilibrium of the contacting phases, and that no phases are generated or depleted over the expected temperature range.

## Synthesis Representation

The representation uses reactor and temperature control units. The *reactors* follow the shadow reactor superstructure by Mehta and Kokossis (1997, 1998). Each *reactor compartment* (a) processes reaction within a particular phase, (b) accommodates mixing through links with other compartments of the same phase, and (c) accounts for mass transfer through its shadow units in other phases. Shadow reactor compartments consist of ideal, homogeneous reactors. The default units include CSTRs and PFRs. Combining different reactor compartments is able to attain an exhaustive array of conventional and novel reactors (Mehta and Kokossis, 1997, 1998).

PFRs are represented by a series of SPFRs (Kokossis and Floudas, 1994a). Unlike Kokossis and Floudas (1994a), however, side streams are included on every sub-CSTR (SCSTR). For multiphase systems, the phase links between PFRs feature the same number of SPFRs. Figure 2 shows the PFR representation adopted in this work. The representation involves $N$ compartments in each of the $NP$ phases. The functions of the compartments are formalized with the use of the following sets:

$P = \{p\}$ moving phases present in the system
$I = \{i\}$ shadow compartments
$Sp = \{s\}$ stream splitters
$SK = \{sk\}$ sub-CSTRs
$I_P^{CSTR} = \{i \mid i \in I$ back-mixed compartment $i$ of phase $p\}$
$I_P^{PFR} = \{i \mid i \in I$ plug-flow compartment $i$ of phase $p\}$
$I_P^{PFR^+} = \{i \mid i \in I$ plug-flow compartment of phase $p$ in direction of reference phase $P^{Ref}\}$

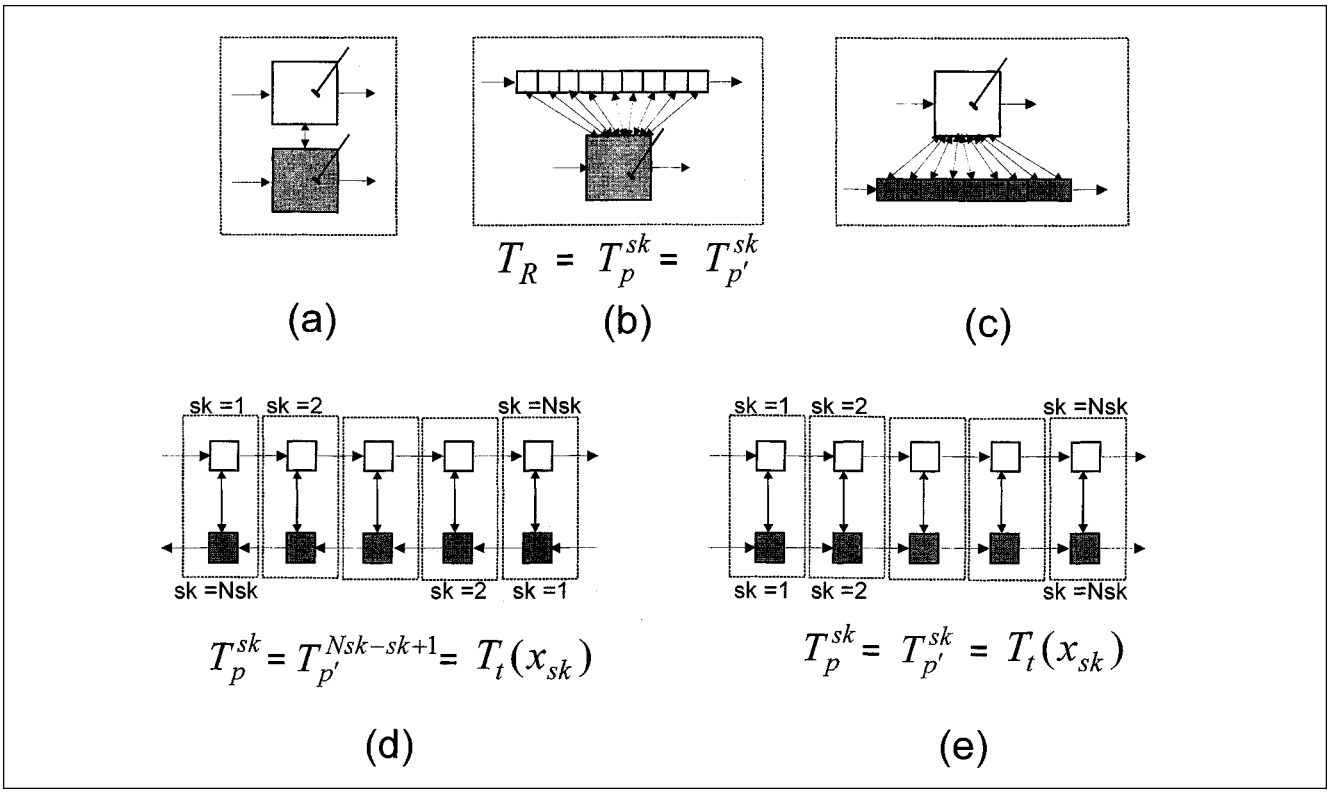


**Figure 3. Control volumes for a two-phase system.**

$I_P^{PFR^-} = \{i \mid i \in I$ plug-flow compartment of phase $p$ in direction opposite to the reference phase $P^{Ref}\}$

$P_i^{CSTR} = \{p \mid p \in P$ phase $p$ in back mixed compartment $i\}$

$P_i^{PFR} = \{p \mid p \in P$ phase $p$ in plug-flow compartment$\}$

$PP^{PFR} = \{i \mid i \in I_p^{PFR} \ \forall p \in P$ multiphase units with shadow compartments as PFR$\}$

Let also,

$ISP_{p,i} = \{isp\}$ be the SPFRs of a PFR, $i \in I_P^{PFR}$, $p \in P$

$ISP_{p,i,isp}^{SK} = \{sk\}$ be the $sk$ SCSTRs assigned to $isp \in ISP_{p,i}$

$ISP_{p,i,isp}^{SK1} = \{sk\}$ be the SCSTR with rank 1 in the cascade

$N_i^{SP}$ = cardinality of set $ISP_{p,i}$.

Control units are used to manipulate temperature changes. The PBS approach requires temperature profiles; the UBS involves heaters and coolers. Due to the assumption of thermal equilibrium, a single temperature is required for each shadow compartment. The two-phase system is illustrated in Figure 3. Temperature profiles account for the contacting phases in the plug flow ($i \in PP^{PFR}$). Each SPFR is assigned to a profile (PBS approach) or a heat exchanger (UBS approach). Let $TP = \{t\}$ be the set of profiles associated with each SPFR. The set includes:

1. Flat or isothermal profiles; they are denoted by $ITP = \{t\}$
2. Monotonic profiles with a concave/convex shape; they are denoted by $CTP = \{t\}$
3. Asymptotic and exponential profiles; they are denoted by $FTP = \{t\}$
4. Nonmonotonic profiles of positive/negative peaks; they are denoted by $PTP = \{t\}$.

The optimization studies of this article all make exclusive use of these four sets. Additional sets can be included, but most complex profiles are possible to develop out of these basic sets. Indeed, the asymptotic profiles in (3) are possible to construct from (1) and (2). Similarly, the flat profiles in (1)

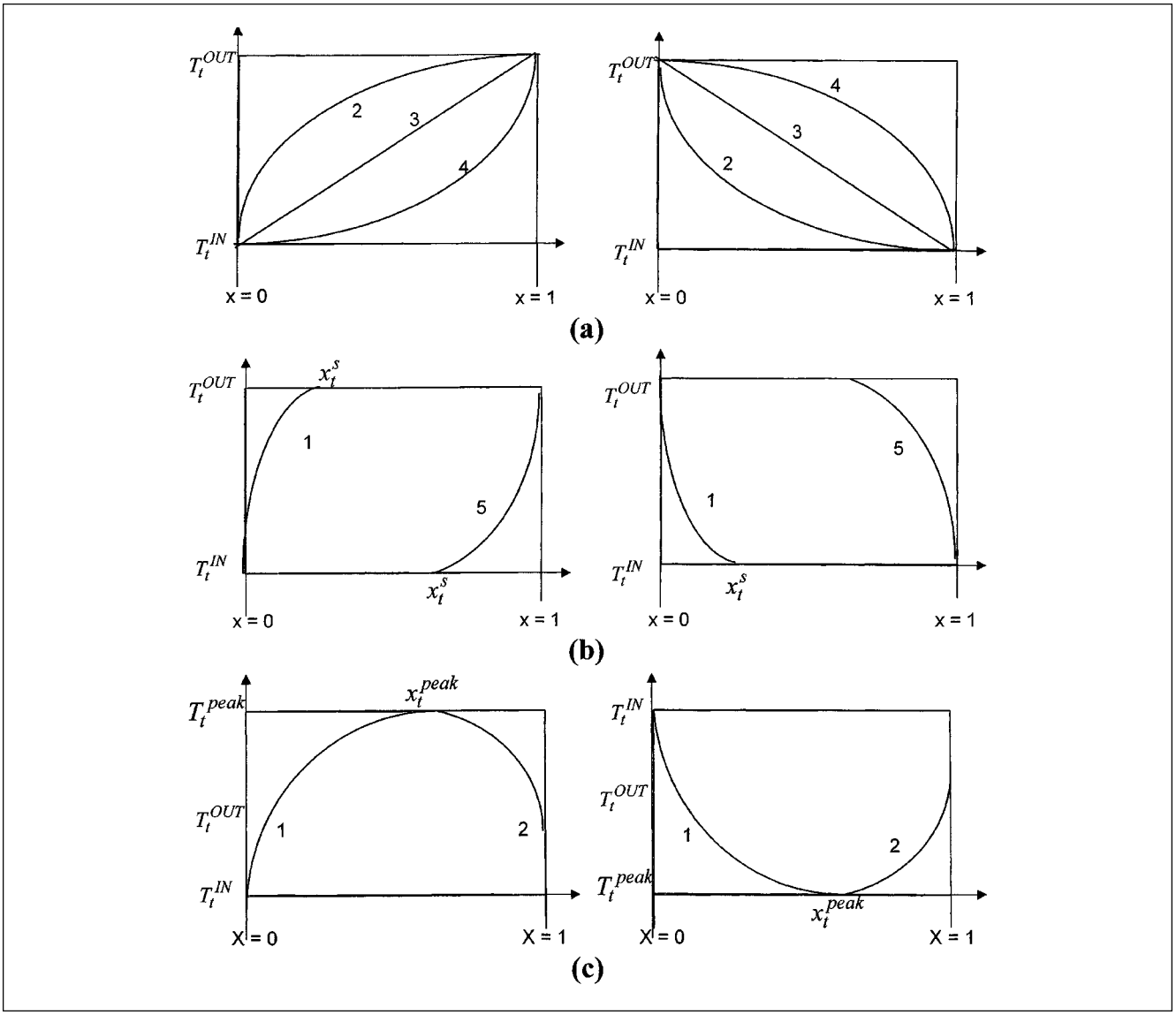


**Figure 4. Basic profiles.**

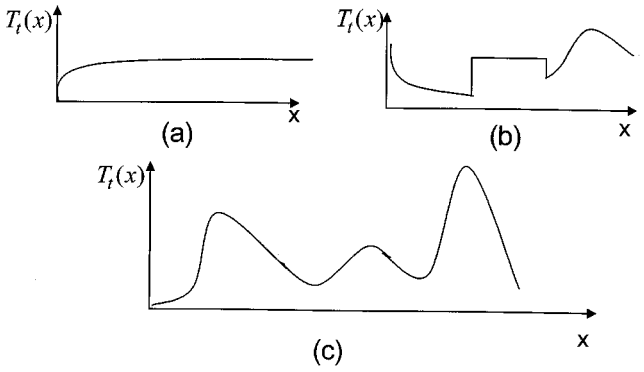


**Figure 5. Special cases of complex profiles.**

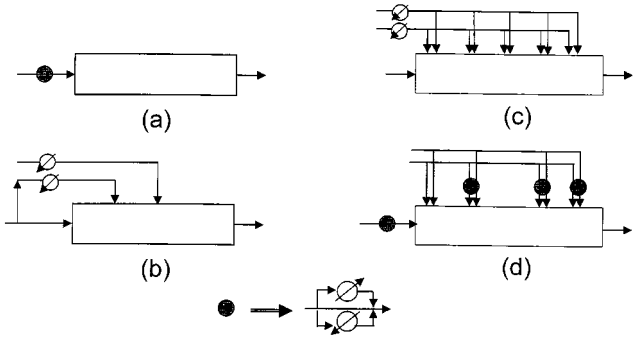


**Figure 6. Representation of nonisothermal PFR.**

can be considered as a special case of the monotonic profiles (2). Figure 4 illustrates examples of each category (Figure 4a: monotonic; Figure 4b: asymptotic and exponential; Figure 4c: peaked profiles). Figure 5a, Figure 5b, and Figure 5c illustrate examples of complex profiles that are possible to construct from the basic sets.

In the alternative UBS approach, the manipulation of the temperature is accomplished with the use of heat-exchanger units. Exchangers can be assigned on every CSTR and PFR following Kokossis and Floudas (1994a). Heaters and coolers are introduced on the inlet stream of each CSTR. Additional heat exchangers for the PFRs are required at (1) the inlet of every SPFR, (2) on every feed stream, and (3) on each SCSTR side stream. Heat exchangers on the side streams define the inlet temperature of the unmixed distributed side streams. Let $HX = \{hx\}$ be the set of network heat exchangers. For each SPFR $isp \in ISP_{p,i}$ heat exchangers (heaters and coolers) relate to the:

$$ISP^{HX}_{p,i,isp} = \{hx \in HX \mid \text{units at the inlet of a SPFR}\}$$

$$S^{HX}_{p,s,i} = \{hx \in HX \mid \text{units on the stream splitter } SSP_{p,s,i},\ s \in S_p\}$$

$$SS^{HX}_{p,s,i,sk} = \{hx \in HX \mid \text{units on side streams from } SSP_{p,s,i},\ s \in S_p \text{ to } sk \in SK\}$$

$$ISC^{HX}_{p,i} = \{hx \in HX \mid \text{units on CSTR inlet of phase } p \in P \text{ and } i \in I^{CSTR}_P\}.$$

The adopted layout is illustrated in Figure 6. The heat duties are used to adjust the inlet temperature of the CSTRs or the inlet temperatures of the PFR side streams.

## Profile Galleries

### *Control parameters*

The characteristic temperatures of profiles include:

$T_t^{\text{in}}$ = inlet profile temperature
$T_t^{\text{out}}$ = outlet profile temperature
$T_t^{\text{Peak}}$ = the peak temperature of the profile.

Temperatures are bounded within $(T_{\min}, T_{\max})$. Let $T_t(x)$ denote the profile over the dimensionless SPFR length $0 \le x \le 1$. Function $T_t(x)$ assumes the general quadratic form $Tq_t(x)$:

$$Tq_t(x) = a_t \cdot x^2 + b_t \cdot x + c_t. \tag{1}$$

Profiles are functions of end temperatures, peak temperatures, and control parameters. These include

For $t \in FTP$, $x_t^s \in (0,1)$ denotes a transition from constant to monotonic profiles.

For $t \in PTP$, $x_t^{\text{Peak}} \in (0,1)$ denotes the position of the peak.

For $t \in TP$, the integer $Ze_t = \{-1, 0, 1\}$ governs the relative position between $T_t^{\text{in}}$ and $T_t^{\text{out}}$.

For $t \in TP$, the integer $Zm_t = \{-1, 1\}$ governs the shape (concave or convex).

For $t \in PTP$, the integer $Zf_t = \{-1, 1\}$ controls the location of flat profiles.

For $t \in PTP$, the integer $Zp_t = \{-1, 1\}$ controls the nature of the peak (positive or negative).

Changes between end temperatures $T_t^{\text{out}}$ and $T_t^{\text{in}}$ are associated with $Ze_t$ as

$$\text{sign}(Ze_t) = \text{sign}\left(T_t^{\text{out}} - T_t^{\text{in}}\right). \tag{2}$$

The value of $Ze_t$ defines the overall temperature progression. For $Ze_t = 1$ there is a temperature increase, whereas for $Ze_t = -1$ there is a temperature decrease. The analytical expressions for the temperature development along a reactor $T_t(x)$ is described separately for each profile.

### *Basic profiles*

1. *Isothermal profiles* are based on $Ze_t = 0$ and $T_t^{\text{in}} = T_t^{\text{out}}$. The assignment of either $T_t^{\text{in}}$ or $T_t^{\text{out}}$ yields

$$T_t(x) = T_t^{\text{in}} = T_t^{\text{out}} \qquad 0 \le x \le 1. \tag{3}$$

2. *Monotonic profiles* are based on

$$0 \le |a_t| \le |T_t^{\text{out}} - T_t^{\text{in}}| \tag{4}$$

$$a_t \cdot Zm_t \ge 0. \tag{5}$$

Given $Ze_t$, $Zm_t$, $T_t^{in}$, and $T_t^{out}$, the profile $T_t(x)$ is given as

$$T_t(x) = \max\left\{T_t^{low}, \min\left(T_t^{high}, Tq_t(x)\right)\right\} \qquad 0 \le x \le 1, \quad (6)$$

where

$$T_t^{low} = \min\left(T_t^{out}, T_t^{in}\right) \quad (7)$$

$$T_t^{high} = \max\left(T_t^{out}, T_t^{in}\right) \quad (8)$$

$$c_t = T_t^{in} \quad (9)$$

$$b_t = T_t^{in}. \quad (10)$$

For $Zm_t = 1$ the profile assumes a convex shape ($a_t \ge 0$) while $Zm_t = -1$ indicates a concave shape ($a_t \le 0$). From Eq. 4, the range of values for $a_t$ excludes peaks along the reactor.

3. *Asymptotic and exponential profiles* are modeled as combinations of curved and flat profiles. Figures 4a and 4b illustrate increasing and decreasing profiles (Profiles 1). Similarly, exponential profiles are modeled as flat profiles combined with steep curves. Figures 4a and 4b illustrate exponential profiles (Profiles 5). In all cases, the curved part of the profile is a quadratic function. Given values for $Ze_t$ $Zf_t$, $x_t^s$, $T_t^{in}$, and $T_t^{out}$, the temperature profile $T_t(x)$ is given by

$$T_t(x) = \max\left\{T_t^{low}, \min\left[T_t^{high}, Tq_t(x)\right]\right\} \quad 0 \le x \le 1, \quad (11)$$

where $T_t^{low}$, $T_t^{high}$, $c_t$, and $b_t$ are given by Eqs. 7 to 10. The parameter $a_t$ is given by

$$a_t = \begin{cases} -\left(T_t^{out} - T_t^{in}\right)/x_t^s & Zf_t = 1 \\ \left(T_t^{out} - T_t^{in}\right)/\left(1 - x_t^s\right) & Zf_t = -1. \end{cases} \quad (12)$$

For $Zf_t = 1$, Eq. 11 yields an asymptotic profile. For $Zf_t = -1$, it yields an exponential profile.

4. *Peaked profiles* involve one additional control parameter $x_t^{Peak}$. Let $T_t^{Peak} = T_t(x_t^{Peak})$. The profiles are based on

$$Zp_t \cdot \left(T_t^{Peak} - T_t^{out}\right) \ge 0 \quad (13)$$

$$Zp_t \cdot \left(T_t^{Peak} - T_t^{in}\right) \ge 0. \quad (14)$$

Given values for $Ze_t$, $Zp_t$, $x_t^{Peak}$, $T_t^{in}$, $T_t^{out}$, and $T_t^{Peak}(x)$, the temperature profile $T_t(x)$ is evaluated using the following quadratic expressions:

$$T_t(x) = \begin{cases} a1_t \cdot x^2 + b1_t \cdot x + c1_t & 0 \le x \le x_t^{Peak} \\ a2_t \cdot x^2 + b2_t \cdot x + c2_t & x_t^{Peak} \le x \le 1. \end{cases} \quad (15)$$

Parameters $a1_t$ $b1_t$, $c1_t$, $a2_t$, $b2_t$, and $c2_t$ are given by:

$$a1_t = -\left(T_t^{Peak} - T_t^{in}\right)/x_t^{Peak} \quad (16)$$

$$a2_t = \left(T_t^{out} - T_t^{Peak}\right)/\left(1 - x_t^{Peak}\right) \quad (17)$$

$$b1_t = -\left(T_t^{Peak} - T_t^{in}\right) - a1_t \quad (18)$$

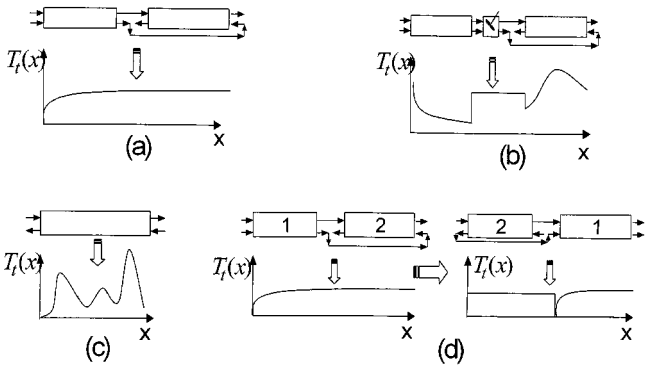


**Figure 7. Temperature profiles.**

$$b2_t = \left(T_t^{out} - T_t^{Peak}\right) - a2_t \quad (19)$$

$$c1_t = T_t^{in} \quad (20)$$

$$c1_t = T_t^{Peak}. \quad (21)$$

Complex profiles are obtained by combining basic profiles. Horizontal shifts are allowed with a control parameter $xs_t \in [-0.5, 0.5]$ introduced on every $t \in TP$. The $T_t(x)$ is given by

$$T_t(x') = \begin{cases} T_t^{in} & 0 \le x' \le \max(0, xs_t) \\ T_t(x) & \max(0, xs_t) \le x' \le \min(1, 1 + xs_t) \\ T_t^{out} & \min(1, 1 + xs_t) \le x' \le 1. \end{cases} \quad (22)$$

Parameters $x' = x + xs_t$ are given by one of Eqs. 6, 11 or 15. Figures 5 and 7 illustrate complex profiles.

## Optimization Framework

Following Mehta and Kokossis (1997), the multiphase reactor network superstructure is optimized using a stochastic optimization approach. The optimization applies simulated annealing. The nonisothermal considerations regard additional moves for the temperature profiles (PBS approach) and the heat-exchanger units (UBS approach).

### *Basic profile moves*

The basic profile moves perturb the characteristic temperatures and the profile shapes. Their steps include the

1. Selection of a shadow reactor compartment $i \in PP^{PFR}$
2. Selection of a SPFR, $isp \in ISP_{p\mathrm{Ref},i,isp}$ in the reference phase $p^{Ref}$
3. Selection of a new profile for the selected SPFR
4. Assignment of temperatures to all the SCSTRs of the SPFR
5. Assignment of temperatures to the contacting phases.

1. *Temperatures changes* involve changes in

(a) *Control parameters* through (1) changes of the parameter; $Ze_t$; (2) recalculation of the characteristic temperatures ($T_t^{in}$, $T_t^{out}$, or $T_t^{Peak}$); (3) recalculation of the coefficients $a_t$, $b_t$, and $c_t$; and (4) evaluation of $T_t(x)$.

(b) *Characteristic temperatures* with (1) a selection of the temperature, ($T_t^{in}$, $T_t^{out}$, or $T_t^{Peak}$) to change; (2) new values

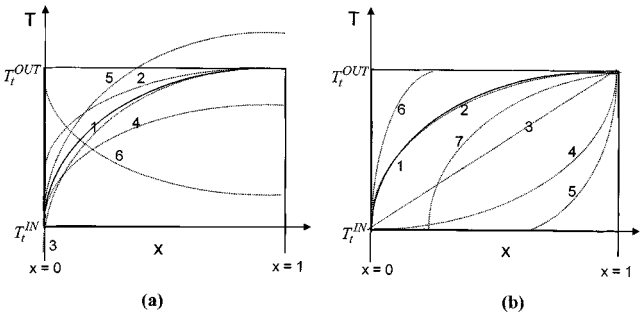


**Figure 8. Perturbation moves.**

for the selected temperature; (3) recalculation of $c_t$ on all the profiles; and (4) evaluation of $T_t(x)$ for the SPFR.

2. *Profile shape changes* involve (1) selection and changes of control parameters $Ze_t$, $Zm_t$, $Zf_t$, $Zp_t$, $x_t^s$, $x_t^{\text{Peak}}$, and $xs_t$; (2) recalculation of $a_t$ (or $a1_t$ and $a2_t$ for peaked profiles) and $b_t$ (or $b1_t$ and $b2_t$ for peaked profiles); and (3) the development of new profiles $T_t(x)$ for the selected SPFR.

Figure 8a illustrates the changes in the characteristic temperatures. They are applied on the base case monotonic Profile 1. New Profiles 2, 3, 4, and 5 are developed from changes to the end temperatures (no change of profile shape), while Profile 6 is generated by swapping inlet and outlet temperatures. Figure 8b illustrates changes of the shape. They are applied to $t \in CTP$. The new profiles are sketched with dotted lines. Changes in the coefficient $a_t$ yield the different Profiles 2 or 3 (linear profiles). Changes to $Zm_t = 1$ are combined with a new coefficient $a_t$ to yield the convex Profile 4, or the Profiles 6 in Figure 8b. A positive shift $x_t^s$ results to Profile 7.

### *Moves on multiple profiles*

The moves on multiple profiles affect more than a single SPFR and include:

1. *Splitting operations* include the following steps: (i) selection of an integer $N1$ and a SPFR, $isp \in ISP_{pRef_{i,isp}}$ in the reference phase, $N^{SP} < N1 \leq Nsk_{i,isp}^{SP}$ (where $N_i^{SP}$ represents the minimum number of SCSTRs); (ii) splitting of first $N1$ SCSTRs as a new SPFR of rank *isp*-1; and (iii) assignment of the existing profile on the new SPFR.

2. *Merging operations* include the following steps: (i) selection of two consecutive SPFRs in the reference phase; (ii) merging of the SCSTRs from both units as a single SPFR; and (iii) assignment of one of the available profiles to the merged unit.

3. *Swapping operations* include the following steps: (i) selection of two SPFRs in the reference phase; (ii) swapping of the characteristic control parameters; and (iii) evaluation of the new profiles for each SPFR.

4. *Mutation operations* include the following steps: (i) selection of a SPFR; (ii) elimination of all other profiles in the PFR; and (iii) assignment of the temperature profile of the selected SPFR to all other SPFRs.

The moves for the heat-transfer units include:

1. *Modification* of heat duties. The moves are accomplished by the manipulation of the outlet temperature. The moves apply to currently existing heat exchangers.

2. *Addition* of a new heat exchangers. The moves introduce new units and apply on existing streams.

3. *Elimination* of heat exchangers. The moves discard existing units from the network.

The implementation of moves employs a temperature discretization. The discrete levels are used to select new temperatures and assign profiles on the PFR. As the PFR is also discretized into SPFRs, the relative position of the SPFR (that is, its rank in the cascade) determines the dimensionless length $x_{sk}$. Kinetic data, as well as thermodynamic and physical parameters are calculated at temperatures selected at the current annealing iteration. *The assignment of profiles diminishes the need for energy balances in the network.* Consequently, the optimization is as difficult as in the isothermal problem; it is certainly much easier than in the UBS approach, where energy balances are required to converge temperatures at each simulation stage. Energy balances are very sensitive to scaling and time consuming.

## Illustration Examples

The new propositions are presented with single and multiphase examples. The single-phase examples (Examples 1–4) explain merits over past studies and conventional synthesis methods. Multiphase examples (Examples 5 and 6) are presented for the first time in the literature. The approach did not require the support of a learning process or an intuitive, repeated use of the methodology. Following the standard procedures of simulated annealing, a set of stochastic runs is required for each case. The standard deviation of the experiments measures the confidence in the optimization. For all examples, the deviation is reported together with the targets. The default superstructure consists of three stages. PFRs consist of 15 SCSTRs and SPFRs of 5 SCSTRs. The number of SPFRs is kept constant and no more than five splits are allowed per PFR per stream. The perturbation probabilities are shown in Table 1. Results emphasize targets and tradeoffs to remain consistent with the functions and purpose of the approach. The runs used an HP9000-C100 workstation.

### *Example 1: Naphthalene oxidation*

This example has been studied by several groups (Chitra and Govind, 1985b; Achenie and Biegler, 1986; Kokossis and Floudas 1994b), each reporting a different solution. The new approach explains the large number of optimal solutions that exist. It further illustrates systematic venues to extract simple layouts. The process is a highly exothermic oxidation:

$$A \xrightarrow{k_1} B \tag{23}$$

$$A \xrightarrow{k_2} C \tag{24}$$

$$B \xrightarrow{k_3} C \tag{25}$$

$$B \xrightarrow{k_4} D \tag{26}$$

*A* stands for naphthalene, *B* for naphthloquinone, *C* for naphthalic anhydride, and *D* for $CO_2 + H_2O$. The oxygen concentration in the mixture is in excess and taken as a constant. The system is homogeneous and the kinetic parame-

**Table 1. Perturbation Probabilities and Biases**

| | Probabilities |
|---|---|
| **Network Moves** | |
| Reactor/stream/swap | 0.5/0.05/0.0 |
| Reactor add/delete/modify/ change type | 0.25/0.15/0.35/0.25 |
| Stream add/delete/modify | 0.3/0.3/0.4 |
| Volume/diameter change | 1.0/0.0 |
| Change mixing pattern/ flow direction | 1.0/0.0 |
| Volume change ($P_{v1}/P_{v2}/P_{v3}$)* | 0.6/0.2 |
| Swap volume/type | 0.35/0.35 |
| Select reactor type 1/2/3/4/5 | 0.25/0.0/0.75/0.0/0.0 |
| Choose CSTR/PFR | 0.25/0.75 |
| Side-stream move | 0.5 |
| Add/delete/merge/split/ modify/shuffle side stream | 0.25/0.25/0.05/0.05/0.2/0.2 |
| **Profile Biases** | |
| Isothermal/increasing/decreasing profile | |
| Case A All profiles allowed | 0.33/0.33/0.34 |
| Case B Only isothermal and increasing profiles | 0.40/0.60/0.00 |
| Case C Only isothermal and decreasing profiles | 0.40/0.00/0.60 |
| Peak/(asymptotic/exponential)/ monotonic | 0.0/0.4/0.6 |
| Positive/negative peak (for peaked profiles) | 0.0/0.0 |
| Exponential/asymptotic (For monotonic profiles) | 0.4/0.6 |
| Linear/quadratic | 0.3/0.7 |
| Convex/concave | 0.5/0.5 |
| **Profile Perturbation Moves** | |
| Profile/SPFR moves | 1.0/0.0 |
| *Profile moves* | |
| Modify/change | 0.7/0.3 |
| a. Modifications | |
| Modify characteristic temperature/shape | 0.5/0.5 |
| Peak temperature/end temperatures | 0.0/1.0 |
| Inlet/outlet temperature | 0.5/0.5 |
| Change isothermal to curved profile | 0.6 |
| Curvature/Position of $x^{st}$/ $x^{peak}$/*Mod* $a_t$ | 0.1/0.3/0.3/0.3 |
| For peaked profiles operate before/after peak | 0.5/0.5 |
| b. Change characteristic temperature/shape | 0.5/0.5 |
| c. Replacements | |
| Swap end temperatures/rotate around end temperature | 0.5/0.5 |
| Imitate/mirror | 0.5/0.5 |
| Horizontal/vertical mirror | 0.5/0.5 |
| Vertical/horizontal shift | 0.45/0.45 |
| Extreme temperature in the discrete point | 0.1 |
| High/low temperature | 0.5/0.5 |
| *SPFR moves* | |
| Merge/split | 0.5/0.5 |
| Merge forward/backward | 0.5/0.5 |
| Split forward/backward | 0.5/0.5 |

*$P_{v1}$: Probability to change volume within $\pm 50\%$; $P_{v2}$: probability to increase reactor volume up to min ($V_{max}$, 10* volume); $P_{v3}$: probability to decrease reactor volume up to max ($V_{min}$, volume/10).

ters, all of first order (De Maria et al., 1961), are shown in Table 2. The feed is pure *A* (1.0 gmol/L), its temperature is 327°C and its flow rate is 1 L/s. The objective is to maximize

**Table 2. Data for Example 1**

| Reaction Parameters | Path 1 | Path 2 | Path 3 | Path 4 |
|---|---|---|---|---|
| Velocity constant (1/h) | $2.0\times10^{13}$ | $2.0\times10^{13}$ | $8.15\times10^{17}$ | $2.1\times10^{5}$ |
| Activation energy (cal/mol) | 38,000 | 38,000 | 50,000 | 20,000 |
| Heat of reaction | −0.12 | −0.43 | −0.36 | −0.74 |

the yield of *C*. The temperature range is [627−927]°C, and the reactor volumes fall within 0.05−2.0 L.

*Targeting approach:* the design target is 0.999 and is found to be with a very convincing standard deviation 0.01%. Figure 9 illustrates some of the numerous solutions (structures $N1-N3$). The networks favor a single PFR that makes use of all different SPFRs. Most optimal profiles are complex. Choices of simpler profiles are possible to discover using the control parameters of the previous section. Figure 10 illustrates alternative solutions that, respectively, use isothermal ($Ze_t = 0$, structure $N6$), isothermal and/or increasing ($Ze_t = 1$, structure $N5$), and isothermal and/or decreasing ($Ze_t = -1$, structure $N4$) profiles. *It is evident that smooth alternatives are available without compromises on the performance*. The UBS approach is tested for comparison. The synthesis objective is identical (yield 0.999; standard deviation 0.001), but the layouts are unnecessarily complicated. From a practical viewpoint, the designs are also unrealistic. The optimal layouts of the UBS approach are shown in Figures 11a−11c: they

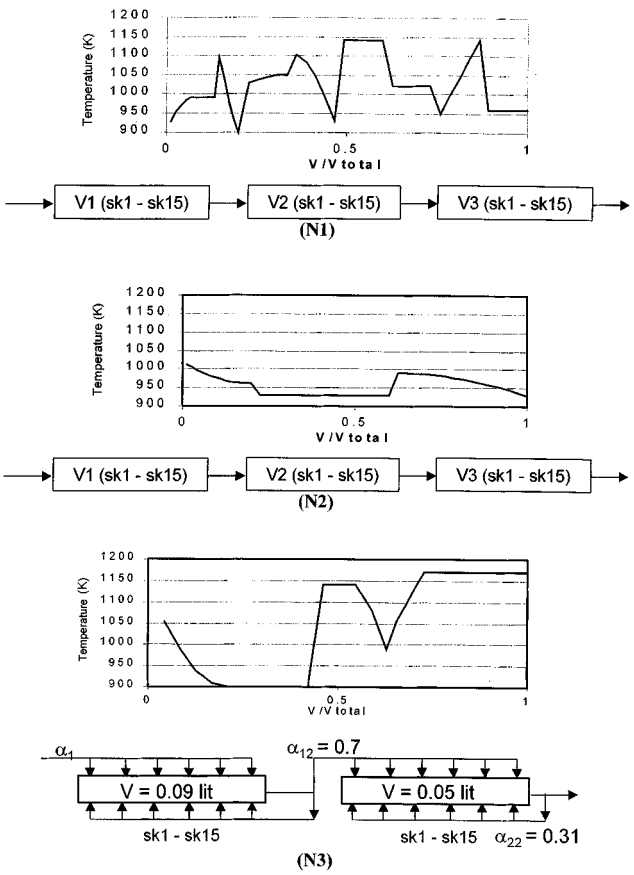


**Figure 9. Results for Example 1 (profile-based search).**

include PFRs with various arrangements of side streams and recycles (integer numbers indicate sub-SCSTRs). Without the control parameters of the profiles, it's highly unlikely simple, practical solutions will be discovered, and the analysis of the design trade-offs is difficult. Using profiles each stochastic run required an average of 1200 function evaluations (3% structures failed to give a converge simulation) and 23 CPU min. Using units, instead, each stochastic run required 2100 function evaluations (26% simulations failed to converge) and 116 CPU min.

### *Example 2: Oxidation of sulphur dioxide*

The merits in using profiles are further explained with a classic example from the literature: the oxidation of sulphur dioxide:

$$SO_2 + 1/2O_2 \overset{r_{SO_2}}{\longleftrightarrow} SO_3. \qquad (27)$$

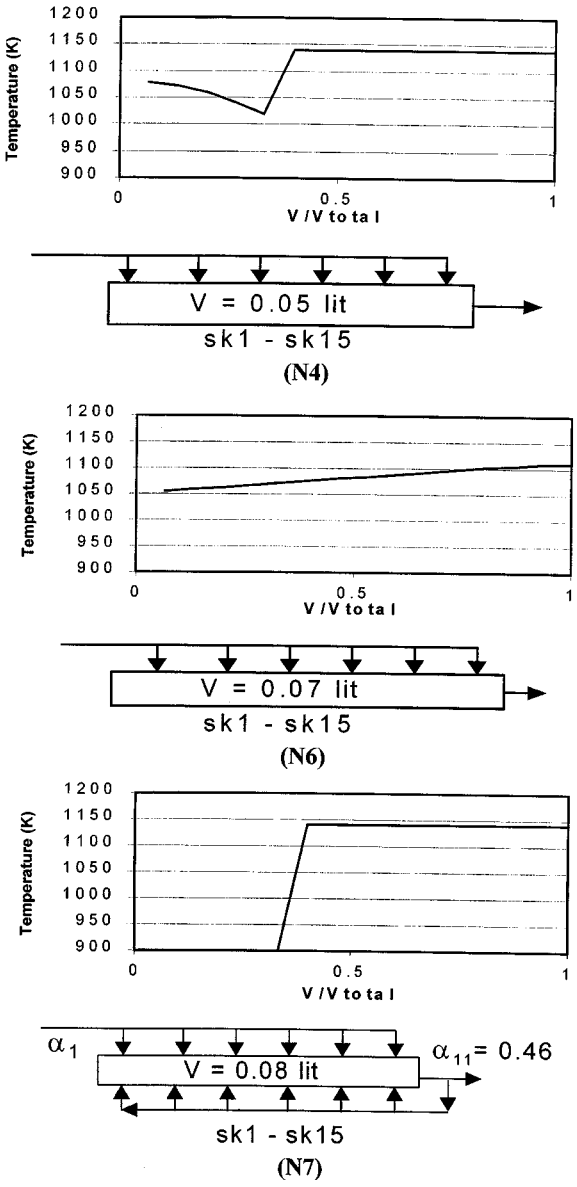


**Figure 10. Results for Example 1 (unit-based search).**

Kinetics on a vanadium catalyst are given by Calderbak (1953):

$$r_{SO_2} = k_1 p_{SO_2}^{1/2} p_{O_2} - \frac{k_2 p_{O_2}^{1/2} p_{SO_3}}{p_{SO_2}^{1/2}}. \qquad (28)$$

The reaction rate is given in terms of kmol of $SO_3$ produced per kg of catalyst per s; the partial and total pressures are in atm. The kinetic constants are

$$k_1 = \exp\left[-31{,}000/R_g T + 12.07\right] \qquad (29)$$

$$k_2 = \exp\left[-53{,}600/R_g T + 22.75\right], \qquad (30)$$

where $R_g$ is the universal gas constant in cal/mol-K, and $T$ the temperature in K. The molar composition of the feed is $SO_3 = 0\%$, $O_2 = 10.42\%$, $SO_2 = 7.51\%$, and $N_2 = 82.05\%$. The feed rate is 7,984 kg/h (19.30 kmols/h of $SO_2$), and its temperature is 37°C; the temperature range is $T$ = [227–727]°C. The objective is the maximization of $SO_3$ for a given maximum catalyst weight ($W_{max}$). Lee and Aris (1963) have reported the first optimization studies. Glasser et al. (1992) reported improvements using attainable region concepts, and Lakshmanan and Biegler (1996) report alternative solutions using MINLP techniques. Balakrishna and Biegler (1992a) studied the process with a similar objective (extent of reaction), to report a decreasing temperature profile and a plug-flow reactor.

*Targeting approach:* the optimization considered a single-stage PFR. Due to the nature of the problem, monotonic isothermal and decreasing profiles are only allowed ($t \in CTP$ with $Ze_t = (0, -1)$). Targets are developed for maximum catalyst loadings between 20 and 40,000 kg ($W1 = 20$ kg, $W2 = 200$ kg, $W3 = 2000$ kg, and $W4 = 40{,}000$ kg). The design target is 10.162 kmol/h ($W_{max} = 20$ kg; standard deviation 1.2%) and 19.3 kmol/h ($W_{max} = 40{,}000$ kg). Solutions are reviewed in Table 3; they explain the increasing yield of $SO_3$ with catalyst weight. Optimal networks are illustrated in Figure 12: they include serial arrangements of PFRs with an occasional assignment of side streams. Figure 13 plots these profiles against the equilibrium curve. The layouts of Figure 12 are to be compared with the layouts obtained from a UBS approach (network constrained to serial structures of PFRs; only feed bypasses are allowed) whose solutions are presented in Figure 14. As with Example 1, the optimization objective is similar but the layout complexity different. Further improvements are trivial to achieve by driving the stochastic results to the nearest KKT points (that is, using NLP optimization). Using profiles required 2500 function evaluations and 37 min. Using profiles instead required 4616 function evaluations (18% failed to converge) and 120 min. With 8–12 runs, the standard deviation dropped below 2%, indicating excellent confidence in the solution quality.

### *Example 3: Van de Vusse reaction (endothermic case)*

The problem is selected to illustrate the impact of the synthesis details on the targeting stage. The optimization runs

**Table 3. Results Summary for Example 2**

| Catalyst Weight (kg) | PBS Approach | | UBS Approach | |
|---|---|---|---|---|
| | $SO_3$ Yield kmol/h | % $SO_2$ Conv. | $SO_3$ Yield kmol/h | % $SO_2$ Conv. |
| $W_{max} = W1 = 20$ | 10.16 | 52.65 | 10.03 | 51.97 |
| $W_{max} = W2 = 200$ | 15.69 | 81.31 | 14.99 | 77.67 |
| $W_{max} = W3 = 2{,}000$ | 18.39 | 95.27 | 18.08 | 93.67 |
| $W_{max} = W4 = 40{,}000$ | 19.26 | 99.80 | 19.24 | 99.67 |

included different reactor representations and different options for the profiles. An endothermic version of the homogeneous van de Vusse is considered:

$$A \xrightarrow{k_1} B \tag{31}$$

$$B \xrightarrow{k_2} C \tag{32}$$

$$A \xrightarrow{k_3} 0.5D. \tag{33}$$

Reaction constants and activation energies are shown in Table 4. The first two reactions are first order; the third one is second order. The synthesis objective is to maximize the yield of *B*. The feed is pure *A* (10 moles/s, concentration 1 mol/L), the temperature range is [177−537]°C, and the volume range is 3.6−600 L.

*Targeting stage:* optimization runs considered cases of a single SPFR or three SPFRs (Table 5). Profile galleries included options of only isothermal and monotonic profiles. The maximum yield ranges within 7.9−8.13 [Kokossis and Floudas (1994) report a similar yield at 7.6]. The results indicate that details in the representation do not affect the optimization (Table 5). The selected designs are shown in Figure 15 and include serial networks of PFRs with occasional recycle and side streams. Networks *P*1, *P*2, and *P*3 result from a single SPFR; networks *PS*1, *PS*2, and *PS*3 are obtained from three SPFRs. The layouts explain similar and consistent trends. For monotonically decreasing profiles as a single option, the isothermal profiles feature an increasing trend. Runs required 2100 function evaluations and 23 min. Figure 16 reviews the designs for cases where units are used instead of profiles (UBS approach); integer numbers indicate sub-SCSTRs. The maximum yield is found to be 8.06 (mean objective is 7.95), and the designs—as is the case of the previous examples—appear to be more complicated. Runs required 4316 function evaluations (6% failed to converge) and 120 min. About 10 runs required to drop the standard deviation below 2%.

### *Example 4: Van de Vusse reaction (exothermic case)*

The optimization experiments of Example 3 are extended for an exothermic version of the Van de Vusse (feed identical

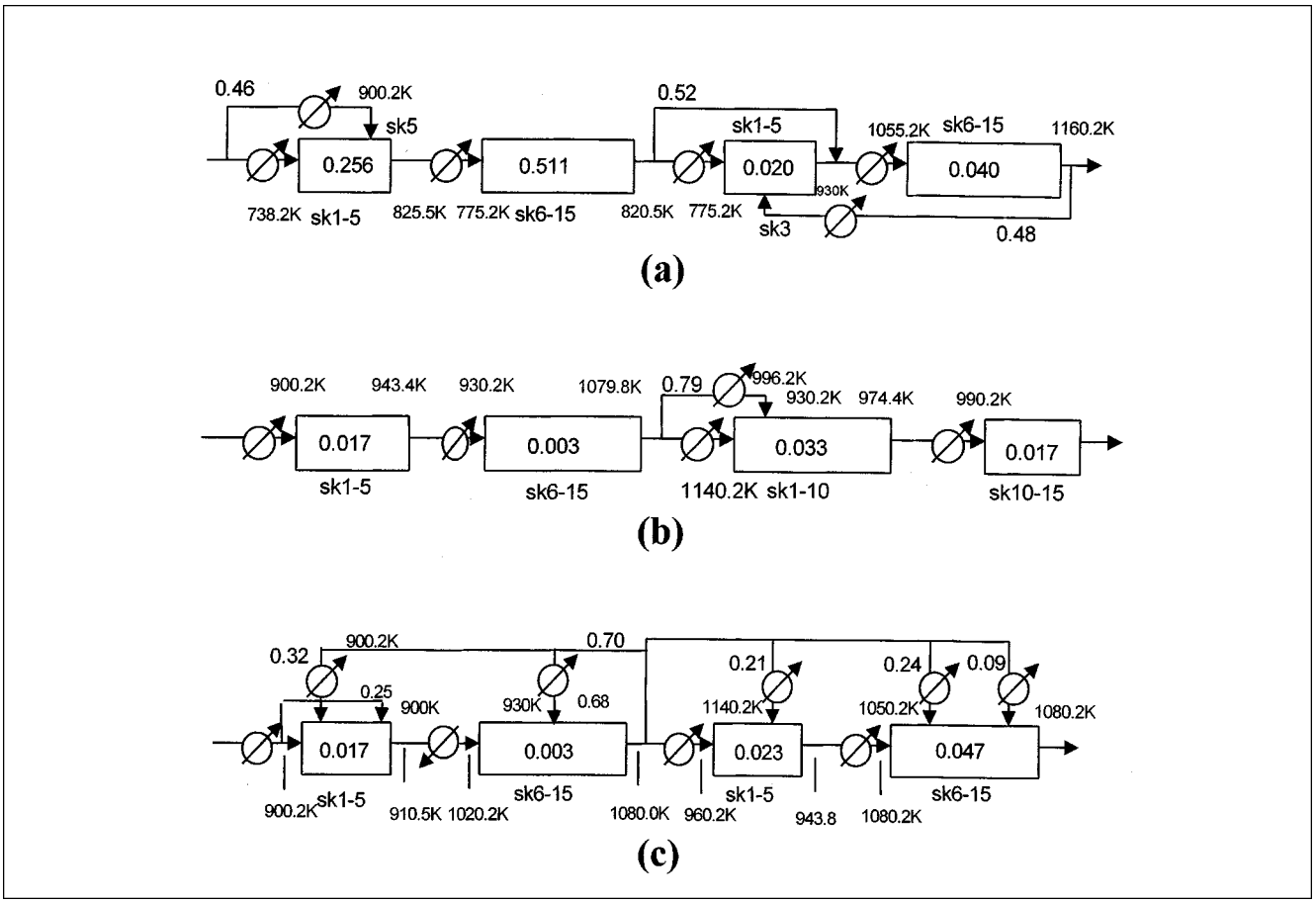


**Figure 11. Adiabatic networks for Example 1 (unit-based search).**

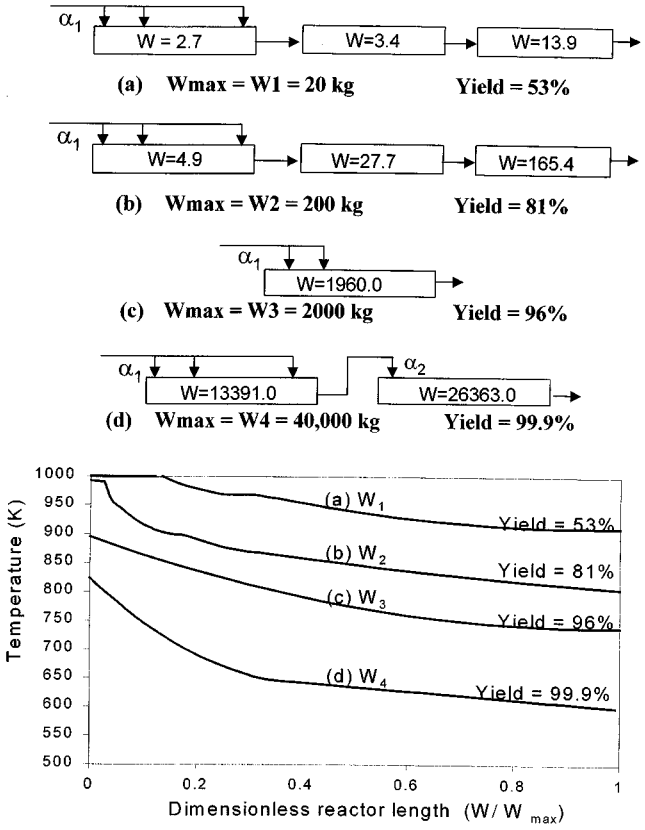


**Figure 12. Results for Example 2 (profile-based search).**

to Example 3). The heat reaction parameters are shown on Table 6. The temperature range is [27–327]°C.

The targeting stage considered:

1. Variable volumes (3.6–100,000 L). The maximum yield is 8.22 (similar to Kokossis and Floudas, 1994a) and favors the decreasing profile of Figure 17a. Optimal networks indicate PFR cascades with side streams; in most cases, the reactor volumes meet their upper bounds. Design *S*1 is an example of an optimal layout.

2. Cases with an upper bound on the volume. For 200 L the yield is 7.65 (all profiles allowed), 7.60 (only increasing profiles), and 7.65 (only decreasing profiles). Optimum profiles are shown in Figure 17b; the optimum structures are similar to Case 1. For 2000 L, the target yield (1 SPFR per PFR) is 8.00 (all profiles allowed), 7.95 (only increasing profiles), and 8.06 (only decreasing profiles). The optimal profiles are shown in Figure 17d. Larger superstructures and differences in the sets of profiles allowed in the search do not alter the targets. A more detailed representation for the PFR also proves pointless. Figure 17c illustrates results where with PFR made up of three SPFRs (upper bound 200 L). The targets change to 7.61 (only increasing profiles), 7.65 (only isothermal or decreasing profiles). Table 7 summarizes the results for further runs.

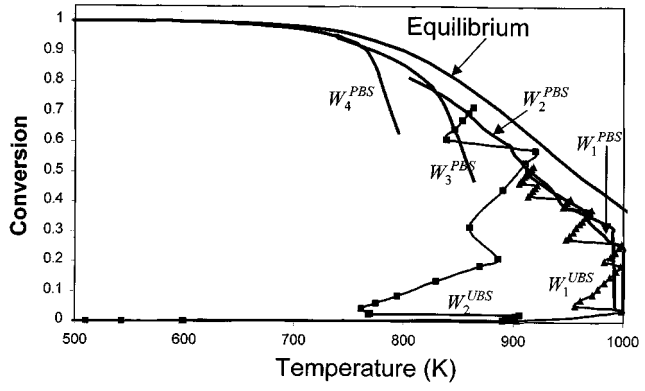


**Figure 13. Optimal profiles for Example 2.**

Optimum profiles and networks are summarized in Table 7 and shown in Figure 17(a)–(d): *P*4–*P*6 (volume 200 L, 3 SPFRs per PFR), *P*7–*P*9 (volume 200 L, 1 SPFR per PFR), *S*4–*S*6 (volume 2,000 L, 1 SPFR per PFR). Each PFR has a maximum of five side streams. Table 7 includes targets and the average values from different stochastic runs. Runs required 2700 function evaluations and 92 min.

For additional layouts obtained by the UBS approach (upper bound for volume at 200 and 2000 L, 3 SPFRs per PFR), the maximum yield is similar to the earlier yields (200 L: 7.56–7.55; 2,000 L: 7.97–7.96). The adiabatic networks are shown in Figure 18: Designs *A*3 and *A*5 (volume 200 L, side streams allowed), *A*4 and *A*6 (2000 L, side streams excluded). Runs required 2900 function evaluations and 241 min. Profiles have again outsmarted the unit-based search and produced simpler designs.

### *Example 5: Multiphase Denbigh (Case A)*

The example is a multiphase version of the Denbigh reaction. A gas–liquid system is assumed, where reactions take place in the liquid phase:

$$A + 2F \xrightarrow{r_1} B + 2H \tag{34}$$

$$A + F \xrightarrow{r_2} D + H \tag{35}$$

$$B + F \xrightarrow{r_3} C + H \tag{36}$$

$$B + 2F \xrightarrow{r_4} E + 2H. \tag{37}$$

Components *A*, *B*, *C*, *D*, and *E* are contained in a nonvolatile liquid phase. Gas-phase component *F* diffuses in the liquid phase, and *H* is a volatile product. The reaction kinetics in the liquid phase are given by

$$r_1 = k_2 \cdot C_{L_A} \cdot C_{L_F} \cdot C_{L_F} \tag{38}$$

$$r_2 = k_1 \cdot C_{L_A} \cdot C_{L_F} \tag{39}$$

$$r_3 = k_3 \cdot C_{L_B} \cdot C_{L_F} \tag{40}$$

$$r_4 = k_4 \cdot C_{L_B} \cdot C_{L_F} \cdot C_{L_F}. \tag{41}$$

**Table 4. Data for Example 3**

| Reaction Parameters | Path 1 | Path 2 | Path 3 |
|---|---|---|---|
| Velocity constant | $5.4\times10^9$ 1/h | $3.6\times10^5$ 1/h | $1.6\times10^{12}$ 1/mol·h |
| Activation energy (cal/mol) | 15,840 | 7,920 | 23,760 |
| Heat of reaction | 0.28 | 0.36 | 0.20 |

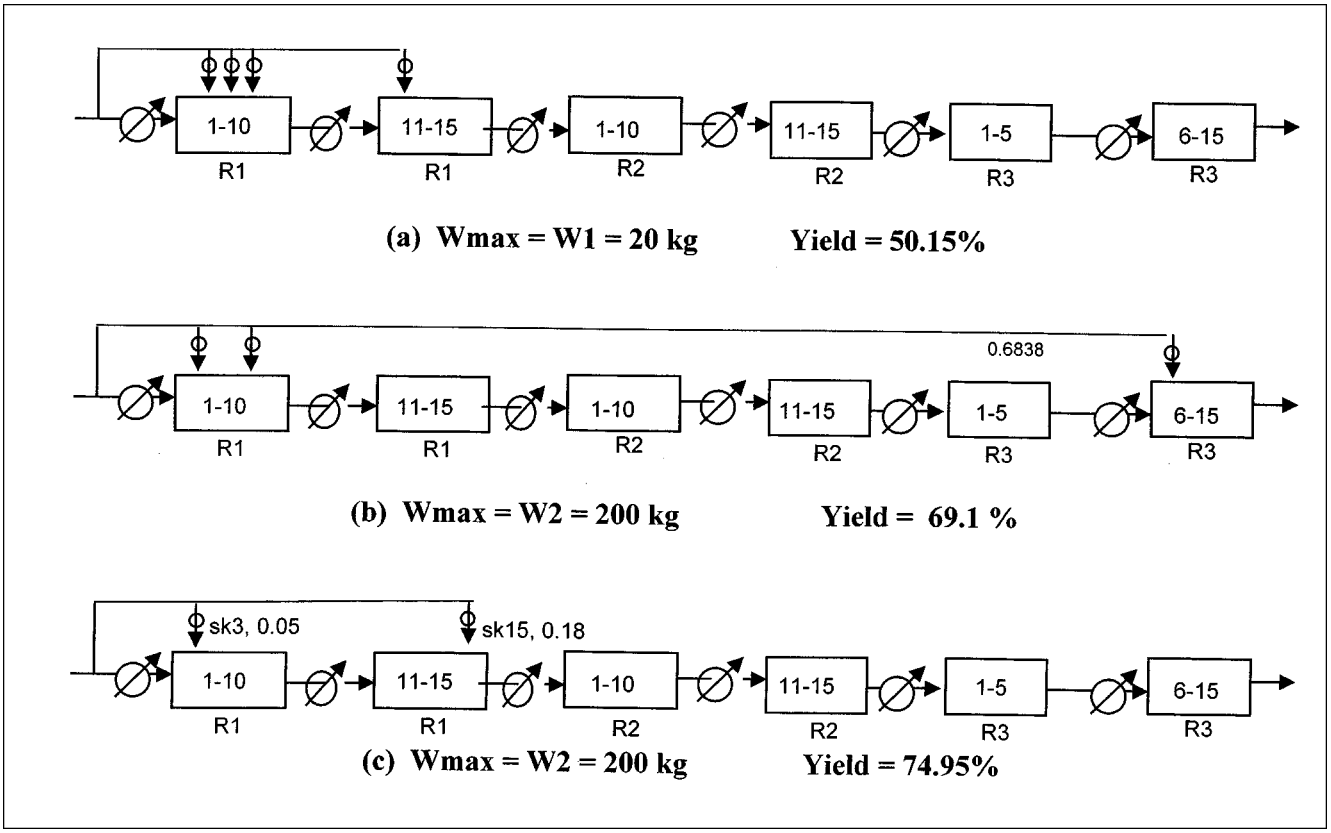


**Figure 14. Results for Example 2 (unit-based search).**

An Arrhenius dependence on temperature is assumed for the Henry constants and the kinetic constants. Kinetic data, preexponential factors, and activation energies are reported in Table 8. For the purposes of the illustration, the effect of temperature on the hydrodynamic parameters is neglected. The volumetric mass-transfer coefficients, the molar-specific volumes for the components in the liquid phase, and the phase holdups are given in Table 9. The volumetric mass-transfer coefficients and the phase holdups are assumed constant for the different types of reactors. The gas and liquid compositions are given in Table 9. The gas flow rate is set to a nominal level. The gas feed has a sparingly soluble inert species *G*, and the liquid feed consists of pure *A*. The objective is to maximize the yield of *B*. Shadow reactor superstructures with three compartments are used. The PFR is represented by cascades of 15 SCSTRs. The bounds on the reactor volumes, the split fractions, and the temperature are given on Table 9. The optimization search excludes combinations of well-mixed gas-phase units with plug-flow liquid-phase units. Up to five unmixed substreams are allowed for each PFR stream.

*Targeting results:* the maximum yield is targeted at 57.7 kmol/h, with a reasonable standard deviation of 2.06%. The selected temperature profile is isothermal and rests at the lower end of the temperature range. The lower temperature increases the solubility of reactant *F* and boosts the rate of the desired reaction. The low temperature decreases the reaction rate of the undesired parallel reaction to product *D*, thus increasing the yield of *B*. Reactor designs are presented

**Table 5. Results Summary for Example 3**

| Allowed Profiles | Network of PFRs Only: 1 SPFR/PFR Mean (max). | Network of PFRs Only: 3 SPFRs/PFR Mean (max.) | General Network: 3 SPFRs/PFR Mean (max.) |
|---|---|---|---|
| | PBS Approach | | |
| → ↑ | 7.98 (8.13) | 7.92 (8.13) | 7.94 (8.13) |
| → ↓ | 7.72 (7.93) | 7.67 (8.07) | — |
| → ↑ ↓* | 7.83 (8.05) | 7.82 (8.10) | 7.95 (8.13) |
| | UBS Approach | | |
| | With side streams (hot/cold shots) | | 7.84 (8.06) |
| | Without side streams (hot/cold shots) | | 7.95 (8.01) |

* →: isothermal profile, ↑: increasing profile, ↓: decreasing profile

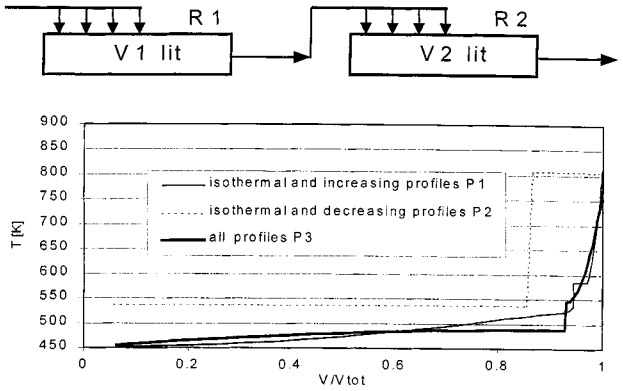


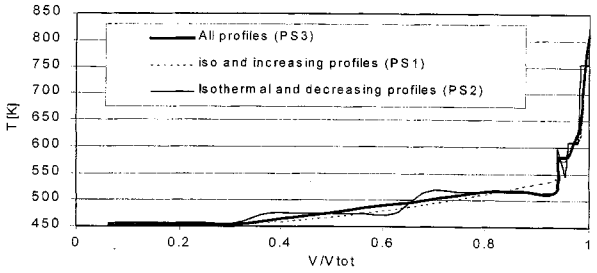


| Structures | Allowed Profiles | V1 lit | V2 lit | Yield |
|---|---|---|---|---|
| P1 | →↑ | 54.8 | 3.6 | 8.04 |
| P2 | →↑ | 21.0 | 3.6 | 7.94 |
| P3 | →↑↓ | 59.4 | 4.7 | 8.05 |
| PS1 | →↑ | 43.8 | 3.6 | 8.13 |
| PS2 | →↑↓ | 46.9 | 3.6 | 8.07 |
| PS3 | →↑↓ | 50.8 | 3.6 | 8.10 |

→ :isothermal profile, ↑: increasing profile, ↓: decreasing profile

**Figure 15. Results for Example 3 (profile-based search).**

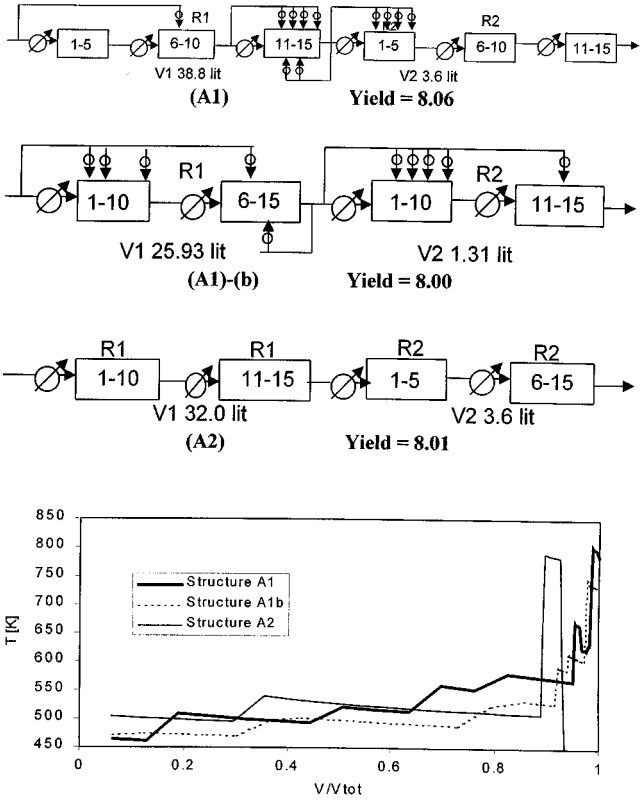


**Figure 16. Results for Example 3 (unit-based search).**

in Figure 19. Designs *S*1 and *S*2 are representative layouts of the selected reactor networks. They indicate a consistent preference for countercurrent reactors. No side streams are observed in the optimal solutions. Runs required about 2700 function evaluations and 92 min.

### *Example 6: Multiphase Denbigh (Case B)*

This example is another multiphase process and a slight variation of Example 5. Kinetics and design parameters follow the description of the previous example. Components *A* and *F* react according to a similar scheme:

$$A + F \xrightarrow{r_1} B + H \tag{42}$$

$$A + 2F \xrightarrow{r_2} D + 2H. \tag{43}$$

The reaction rates are given by

$$r_1 = k_1 \cdot C_{L_A} \cdot C_{L_F} \tag{44}$$

$$r_2 = k_2 \cdot C_{L_A} \cdot C_{L_F} \cdot C_{L_F}. \tag{45}$$

Mass-transfer coefficients, specific molar volumes, phase holdups, Henry's constants, and reaction constants follow the description of Example 5.

*Targeting stage:* the optimal yield is 96.38 (standard deviation 0.4%). The optimal temperature profile is isothermal, but now rests at the *higher end of the temperature range*. The optimal reactor networks include arrangements of cocurrent reactors or combinations of cocurrent and countercurrent reactors. The reactor volumes usually reach their upper bounds (2,000 $m^3$). Designs *S*3 and *S*4 of Figure 20 are representative cases of the selected layouts. Although very similar to Example 5, the reaction process features different trade-offs and the optimization results are contrasting. The differences are explained in the way the temperature affects the solubility and the reaction rates. At higher temperature, the solubility of the gas-phase reactant *F* is lower and the reaction rate to D is higher. The optimization explains that higher temperatures should be used in order to diminish the reactant in the liquid phase and suppress the undesired reaction. The computational effort is similar to the one reported for Example 5.

**Table 6. Data for Example 4**

| Reaction Parameters | Path 1 | Path 2 | Path 3 |
|---|---|---|---|
| Velocity constant | $5.4\times10^9$ 1/h | $1.6\times10^{12}$ 1/h | $3.6\times10^5$ 1/mol·h |
| Activation energy (cal/mol) | 15,840 | 23,760 | 7,920 |
| Heat of reaction | −0.28 | −0.36 | −0.20 |

*Example 7: An industrial case*

The illustrations conclude with an industrial study. The components are concealed as *A*, *B*, *C*, *D*, *E*, *F*, *G*, *H*, *I*, and *J*. The feed consists of *A* and *J*. The product is *B*. The feed rate of *A* is 100.0 kmol/h. The feed ratio is fixed at 6.2 (specification imposed by the engineers). Feeds *A* and *J* are allowed to distribute and are not premixed. The objective is to maximize the product yield. The weight of catalyst per network unit ranges between 1350 to 50,000 kg. The network is constrained to a maximum of four units. The reactions are described by

$$A \xleftrightarrow{r_1} E + B \tag{46}$$

$$A \xrightarrow{r_2} C + G \tag{47}$$

$$A \xrightarrow{r_3} D + F \tag{48}$$

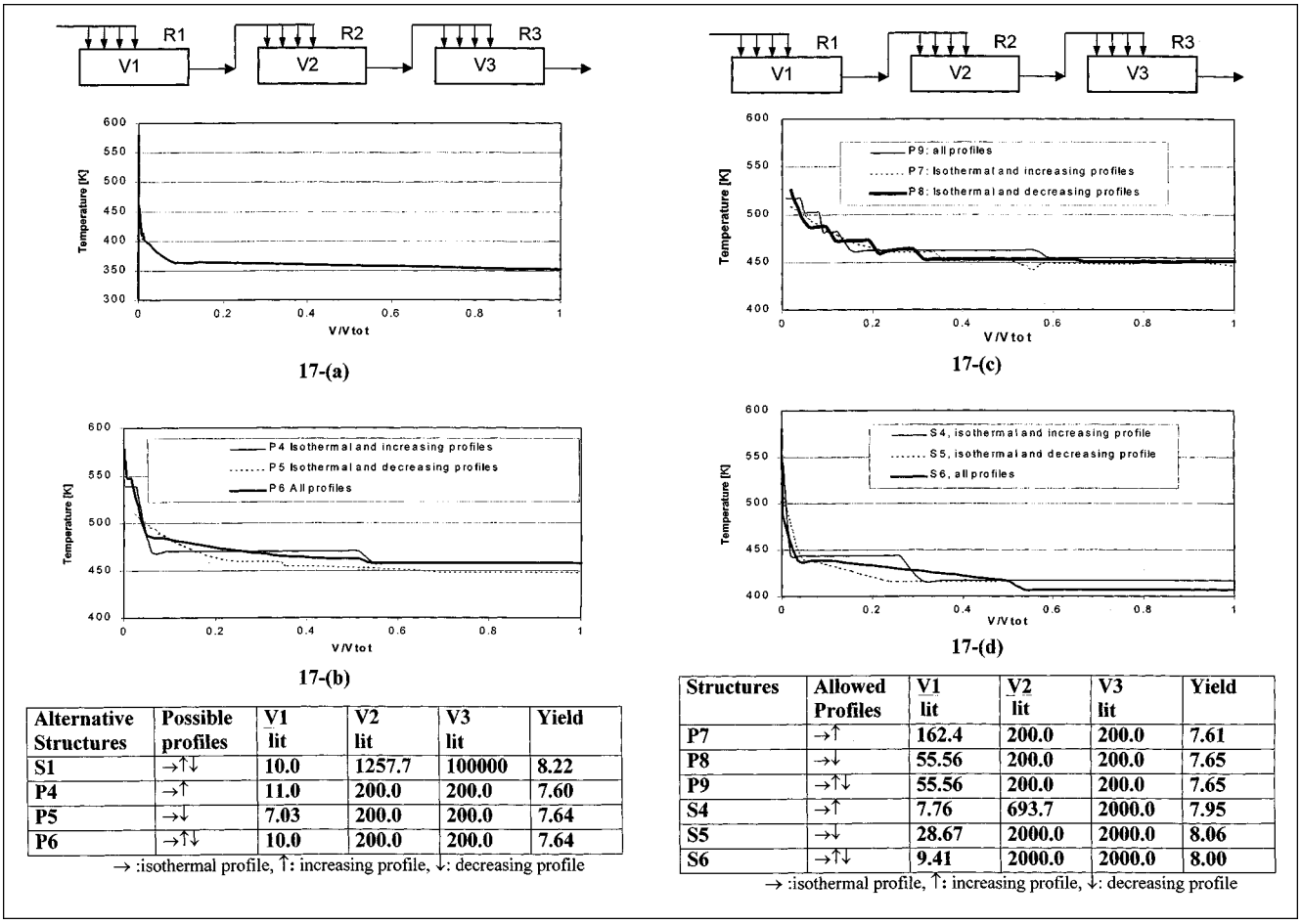


| Alternative Structures | Possible profiles | V1 lit | V2 lit | V3 lit | Yield |
|---|---|---|---|---|---|
| S1 | →↑↓ | 10.0 | 1257.7 | 100000 | 8.22 |
| P4 | →↑ | 11.0 | 200.0 | 200.0 | 7.60 |
| P5 | →↓ | 7.03 | 200.0 | 200.0 | 7.64 |
| P6 | →↑↓ | 10.0 | 200.0 | 200.0 | 7.64 |

→ :isothermal profile, ↑: increasing profile, ↓: decreasing profile

| Structures | Allowed Profiles | V1 lit | V2 lit | V3 lit | Yield |
|---|---|---|---|---|---|
| P7 | →↑ | 162.4 | 200.0 | 200.0 | 7.61 |
| P8 | →↓ | 55.56 | 200.0 | 200.0 | 7.65 |
| P9 | →↑↓ | 55.56 | 200.0 | 200.0 | 7.65 |
| S4 | →↑ | 7.76 | 693.7 | 2000.0 | 7.95 |
| S5 | →↓ | 28.67 | 2000.0 | 2000.0 | 8.06 |
| S6 | →↑↓ | 9.41 | 2000.0 | 2000.0 | 8.00 |

→ :isothermal profile, ↑: increasing profile, ↓: decreasing profile

**Figure 17. Results for Example 4 (profile-based search).**

**Table 7. Results Summary for Example 4**

| | $V_{max}$ = 200 lit | | | | $V_{max}$ = 2,000 lit | | | |
|---|---|---|---|---|---|---|---|---|
| | 1 SPFR/PFR | | 3 SPFRs/PFR | | 1 SPFR/PFR | | 3 SPFRs/PFR | |
| | Mean | Max. | Mean | Max. | Mean | Max. | Mean | Max. |
| | | | PBS Approach | | | | | |
| → ↑ | 7.55 | 7.59 | 7.56 | 7.61 | 7.77 | 7.95 | 7.88 | 8.01 |
| → ↓ | 7.63 | 7.65 | 7.63 | 7.65 | 7.92 | 8.06 | 7.91 | 8.02 |
| → ↑ ↓* | 7.62 | 7.65 | 7.59 | 7.65 | 7.90 | 8.00 | 7.91 | 8.04 |
| | | | UBS Approach | | | | | |
| With side streams | | | 7.37 | 7.56 | | | 7.71 | 7.97 |
| Without side streams | | | 7.48 | 7.55 | | | 7.86 | 7.96 |

* →: isothermal profile, ↑: increasing profile, ↓: decreasing profile; for PBS approach, side streams were allowed in all the cases.

**Table 8. Data for Examples 5 and 6**

| Reaction Parameters | Path 1 | Path 2 | Path 3 | Path 4 |
|---|---|---|---|---|
| Velocity constant $\times 1.0 \times 10^{-4}$ ($m^3$kmol·h) | 540,000.00 | 53.00 | 4.40 | 4.58 |
| Activation energy (cal/mol) | 15,840 | 23,760 | 23,760 | 8,500 |
| Equilibrium parameters (Henry's constant) | Component F | | Component G | |
| Velocity constant $\times 1.0^{-5}$ | 2.20 | | 2.20 | |
| Heat of solubility (cal/mol) | 7,920.00 | | 7,920.00 | |

**Table 9. Problem Data for Examples 5 and 6**

| | |
|---|---|
| *Feed and reaction conditions* | |
| Gas feed (kmol/h) | $F = 200.0$, $G = 800.0$, $H = 0.0$ |
| Liquid feed (kmol/h) | Pure $A = 100$ |
| | $B = C = D = E = F = H = 0$ |
| *Pressure (bar)* | 10.0 |
| Hydrodynamics | |
| Mass transfer coefficients | $K_{la_F} = 500$ |
| (per unit gas vol.) (1/h) | $K_{la_H} = 500$ |
| | $K_{la_G} = 0$ |
| Molar specific volumes for liquid | $V_{sp_A} = V_{sp_B} = 1.6667$ |
| phase ($m^3$/kmol) | $V_{sp_C} = V_{sp_D} = V_{sp_E} = 1.6667$ |
| | $V_{sp_F} = V_{sp_H} = 0$ |
| Liquid phase | $\phi_L = 0.5$ |
| Holdup | (for all reactor types) |
| Bounds | |
| Volume bounds ($m^3$) | $V_{\min} = 10$, $V_{\max} = 2{,}000$ |
| Temperature bounds (K) | $T_{\min} = 300$, $T_{\max} = 600$ |

$$J + 0.5G \xrightarrow{r_4} 2E + I \tag{49}$$

$$J + F \xrightarrow{r_5} 3E + I \tag{50}$$

$$J + I \xrightarrow{r_6} E + H. \tag{51}$$

The gas-phase reactions are catalyzed by solid catalyst and the kinetics are given by

$$r_1 = \frac{k_1 P_A - \dfrac{P_A P_E}{K_{E1}}}{P_A + (K_A + P_B)^2} \tag{52}$$

$$r_2 = \frac{A_1 k_2 P_A}{P_A + (K_A + P_B)^2} \tag{53}$$

$$r_3 = \frac{A_1 k_3 P_A}{P_A + (K_A + P_B)^2} \tag{54}$$

$$r_4 = k_4 K_4 P_G \tag{55}$$

$$r_5 = k_5 K_5 P_F \tag{56}$$

$$r_6 = k_6 K_6 \left( P_J P_I - \frac{P_H P_E}{K_{E6}} \right). \tag{57}$$

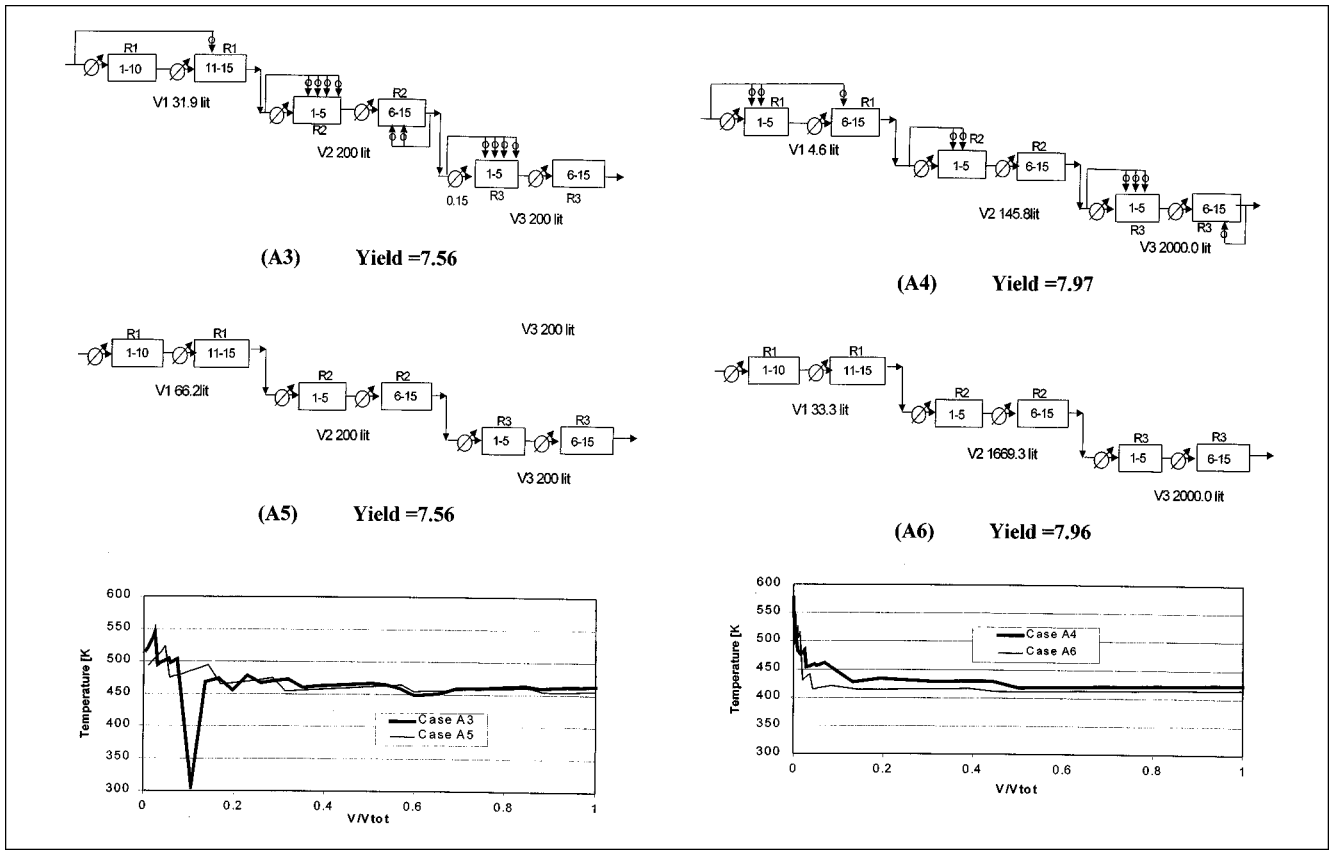


**Figure 18. Results for Example 4 (unit-based search).**

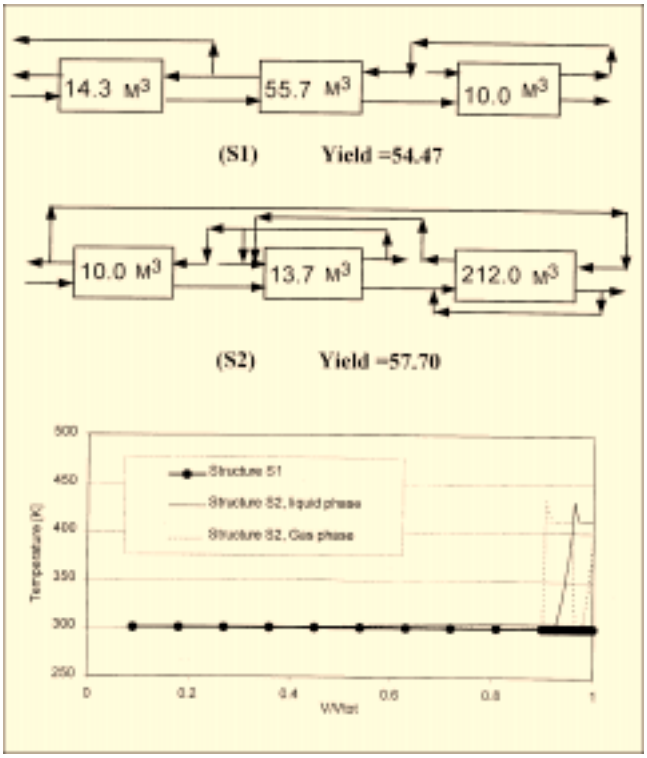


**Figure 19. Results for Example 5 (profile-based search).**

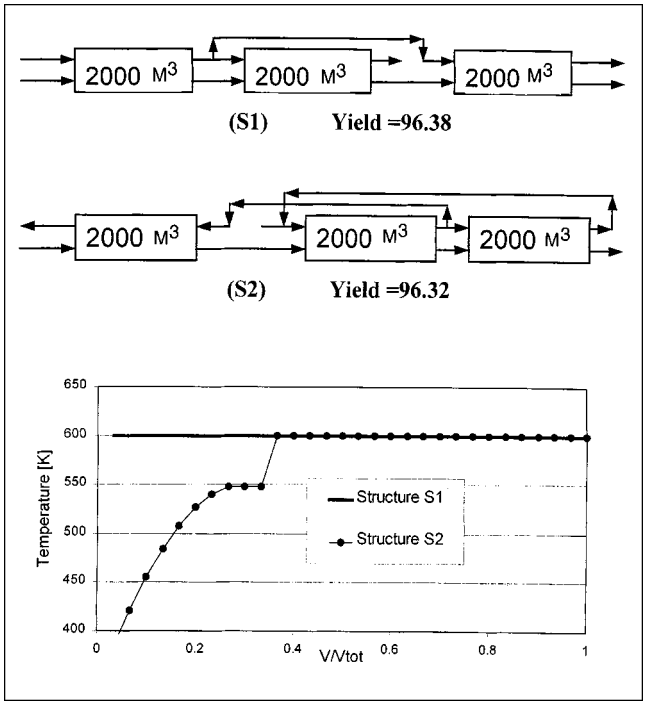


**Figure 20. Results for Example 6 (profile-based search).**

The kinetic constants are described by Arrhenius expressions,

$$ki = A_i \exp\left( A1_i - E_i/R_g T \right). \qquad (58)$$

The kinetic parameters are given in Table 10. The optimization results are shown for the:

1. *Isothermal case* (flat temperature profiles at 843 K). The maximum yield is 85.4 kmol/h. Optimal structures strongly favored a single PFR with a total catalyst of 200,000 kg (upper bound). No side stream distribution is required.

2. *Nonisothermal case*. The temperature is allowed to vary between 800 and 1,000 K. The maximum yield is increased to 96.3. A smooth increasing profile is found to be the optimal. The favored structure is a single PFR. The solution is shown in Figure 21. As in the previous case, no stream distribution is required.

A set of separate isothermal studies were launched to study the optimal feed ratio between $A/J$. The ratio varied within 1−12; in all cases it settled at its upper bound. The optimal structure remained the single PFR (its volume also at upper bound). At 843 K the optimal improved to 94.4. The optimization required 190 min and 3,600 function evaluations. Real-life problems, such as the one presented here, typically require development times that are of several orders of magnitude higher. The optimization technology of this article can thus reduce the effort in a dramatic fashion.

## Conclusions

This article presents a systematic methodology for the synthesis of nonisothermal reactor networks. The approach is generic and there has not been a need to customize the optimization runs. Results are consistently obtained using the biases of Table 1. No particular studies preceded the biases proposed in Table 1. Thus, the authors expect similar results with alternative probabilities. The work addresses major challenges relating to the numerous local optima, the large number of near-optimal alternatives, and the proliferation of solutions in the superstructure models. The article outlines an approach that claims merits at all fronts. It presents a method that is applicable to both homogeneous and multiphase systems. The synthesis framework employs a superstructure embracing temperature profiles rather than heat-transfer units. The selection of the profiles is not unique. As discussed in the third section, one can alternatively employ a different set of profiles. The optimization models are as expensive as the isothermal ones. Furthermore, their control parameters can be used to command simplicity and eliminate redundant searches.

Results are presented for six different problems. The first four examples are simple studies of homogeneous systems. Several research groups have claimed the development of particular layouts as optimal solutions. This work explains that there exist numerous—if not infinite—equivalent solutions. Example 1 is the typical illustration of this argument. It involves simple reactions with first-order kinetics, but its complexity is enough to yield numerous optimal and near-optimal solutions. A much larger number of layouts correspond to local and inferior optima. The approach of this article enables us to (1) reliably review the optimal options, and (2) systematically imply search controls to identify the simplest available alternatives. An additional benefit relates to significant speedups in the optimization. As a rough average, the optimization search based on units requires three times more CPU time to converge than the one based on profiles.

**Table 10. Data for Example 7**

| Reaction Parameter | Ai | Ali | Ei (kcal/kmol) |
|---|---|---|---|
| $k_1$ | 2.000 | 38.10 | 65,900.0 |
| $k_2$ | 0.100 | 39.00 | 74,900.0 |
| $k_3$ | 0.200 | 47.90 | 87,400.0 |
| $k_4$ | 0.874 | 0.00 | 8,779.5 |
| $k_5$ | 0.158 | 0.00 | 8,779.5 |
| $k_6$ | 2.000 | 16.88 | 9,724.1 |
| $K_4$ | 127.0 | 0.00 | 0.0 |
| $K_5$ | 127.0 | 0.00 | 0.00 |
| $K_6$ | $3.1\times10^{-5}$ | 0.00 | 0.0 |
| $K_{E1}$ | 1.000 | 16.12 | 15,350.0 |
| $K_{E6}$ | 1.000 | −4.33 | 909.7 |
| $K_A$ | 100.0 | 0.00 | 0.00 |

An industrial problem is reported for the first time. It consists of 10 components and 6 reactions of the general type. Structures and operational variables are optimized within a few hours. The total time—to set up the problem, prepare physical and kinetic data, make adjustments to the input files, accommodate for process constraints, run the optimization—required a couple of days. The typical times to study —not necessarily optimize—these problems are longer at least by an order of magnitude. The technology thus shows a clear advantage in reducing the total development time. Examples 5 and 6 are also new examples in the literature. They present multiphase systems that process complex reactions. The multiphase examples demonstrate the potential of the methodology to handle more difficult and complex problems. As in the homogeneous case, the approach calculates the optimal performance and discloses the appropriate reactor types to employ.

## Acknowledgments

The authors acknowledge the joint financial support provided by EPSRC (GR/L10105 and GR K91958), the Overseas Research Council, and the Department of Process Integration at UMIST. They acknowledge support by Mr. Patrick Linke who has helped with the preparation of the manuscript.

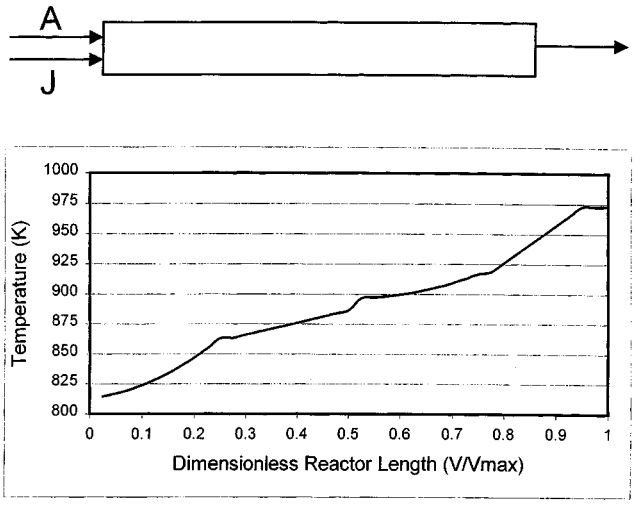


**Figure 21. Results for Example 7 (profile-based search).**

## Notation

### *Sets*

$C$ = concentration
$ic, jc$ = compartments as CSTRs
$ip, jp$ = compartments as PFRs
$I^{CSTR}$ = shadow compartments in CSTR
$I^{PFR}$ = shadow compartments in PFR
$I^{PFR+}$ = shadow compartments in PFR with flow direction same as reference phase
$I^{PFR-}$ = shadow compartments in PFR with flow direction opposite to the reference phase
$L, 1$ = liquid phase
$P^{CSTR}$ = moving phases with shadow compartments as CSTR
$P^{PFR}$ = moving phases with shadow compartments as PFR
$P, p$ = moving phase
$S, s$ = stream splitter
$TP$ = temperature profiles

### *Indices/subscripts*

$F, f$ = feed
$G, g$ = gas phase
$P$ = partial pressure
$T_p$ = temperature of phase $p$
$T_R$ = temperature of multiphase reactor
$x$ = dimensionless PFR length
$x^s$ = dimensionless transition position for flat profiles
$x^{\text{peak}}$ = dimensionless position of a temperature peak
$x_s$ = variable controlling the horizontal shift of temperature profile
$\alpha_{ij}$ = split fraction from compartment $i$ to compartment $j$
$\alpha s_{ijsk}$ = side-stream split fractions for stream from compartment $i$ to compartment $j$ to each of the $sk^{th}$ SCSTRs of compartment $j$

## Literature Cited

Achenie, L. K. E., and L. T. Biegler, ''Algorithmic Synthesis of Chemical Reactor Networks Using Mathematical Programming,'' *Ind. Eng. Chem. Fundam.*, **25**, 621 (1986).Achenie, L. K. E., and L. T. Biegler, ''Developing Targets for the Performance Index of a Chemical Reactor Network: Isothermal Systems,'' *Ind. Eng. Chem. Res.*, **27**, 811 (1988).

Achenie, L. K. E., and L. T. Biegler, ''Superstructure Based Approach to Chemical Reactor Network Synthesis,'' *Comput. Chem. Eng.*, **14**, 23 (1990).

Aris, R., ''On Denbigh's Optimum Temperature Sequence,'' *Chem. Eng. Sci.*, **12**, 56 (1960a).

Aris, R., ''Studies on Optimization: I. The Optimum Design of Adiabatic Reactors with Several Beds,'' *Chem. Eng. Sci.*, **12**, 243 (1960b).

Aris, R., ''Studies on Optimization: II. Optimum Temperature Gradients in Tubular Reactors,'' *Chem. Eng. Sci.*, **13**, 18 (1960c).

Aris, R., ''Studies on Optimization: III. The Optimum Operating Conditions in Sequence of Stirred-Tank Reactors,'' *Chem. Eng. Sci.*, **13**, 75 (1960d).

Aris, R., ''Optimal Bypass Rates for Sequences of Stirred-Tank Reactors,'' *Can. J. Chem. Eng.*, 121 (1961a).

Aris, R., ''Studies on Optimization: IV. The Optimum Conditions for a Single Reaction,'' *Chem. Eng. Sci.*, **13**, 197 (1961b).

Aris, R., ''On Optimal Adiabatic Reactors of Combined Types,'' *Can. J. Chem. Eng.*, 87 (1962).

Aris, R., *Discrete Dynamic Programming*, Blaisdell, New York (1964).

Balakrishna, S., and L. T. Biegler, ''Constructive Targeting Approaches for the Synthesis of Chemical Reactor Networks,'' *Ind. Eng. Chem. Res.*, **31**, 300 (1992a).

Balakrishna, S., and L. T. Biegler, ''Targeting Strategies for the Synthesis and Energy Integration of Nonisothermal Reactor Networks,'' *Ind. Eng. Chem. Res.*, **31**, 2152 (1992b).

Balakrishna, S., and L. T. Biegler, ''A Unified Approach for the Simultaneous Synthesis of Reaction, Energy and Separation Systems,'' *Ind. Eng. Chem. Res.*, **32**, 1372 (1993).

Calderbank, P. H., ''Contact-Process Converter Design,'' *Chem. Eng. Prog.*, **49**, 585 (1953).

Chitra, S. P., and R. Govind, ''Synthesis of Optimal Serial Reactor Structurees for Homogeneous Reactions: I. Isothermal Reactors,'' *AIChE J.*, **31**, 177 (1985a).
Chitra, S. P., and R. Govind, ''Synthesis of Optimal Serial Reactor Structurees for Homogeneous Reactions: II. Nonisothermal Reactors,'' *AIChE J.*, **31**, 185 (1985b).
De Maria, A., J. E. Longfield, and G. Butler, ''Catalyst Reactor Design,'' *Ind. Eng. Chem.*, **17**, 163 (1961).
Dyson, D. C., and J. M. Horn, ''Optimum Distributed Feed Reactors for Exothermic Reversible Reactions,'' *J. Optimiz. Theory Appl.*, **1**, 40 (1967).
Dyson, D. C., J. M. Horn, R. Jackson, and C. B. Schlesinger, ''Reactor Optimisation Problems for Reversible Exothermic Reactions,'' *Can. J. Chem. Eng.*, **45**, 310 (1967).
Dyson, D. C., and J. M. Horn, ''Optimum Adiabatic Cascade Reactor with Direct Intercooling,'' *Ind. Eng. Chem. Fundam.*, **8**, 49 (1969).
Feinberg, M., and J. M. Horn, ''Dynamics of Open Chemical Systems and the Algebraic Structure of the Underlying Reaction Network,'' *Chem. Eng. Sci.*, **29**, 775 (1974).
Glasser, B., D. Hildebrandt, and D. Glasser, ''Optimal Mixing for Exothermic Reversible Reactions,'' *Ind. Eng. Chem. Res.*, **31**, 1541 (1992).
Glasser, D., and D. Hildebrandt, ''Reactor and Process Synthesis,'' *Comput. Chem. Eng.*, **21**, S775 (1997).
Glasser, D., D. Hildebrandt, and C. Crowe, ''Geometric Approach to Steady Flow Reactors: The Attainable Region and Optimization in Concentration Space,'' *Ind. Eng. Chem. Res.*, **26**, 1803 (1987).
Glasser, D., D. Hildebrandt, and S. Godorr, ''The Attainable Region for Segregated, Maximum Mixed, and Other Reactor Models,'' *Ind. Eng. Chem. Res.*, **33**, 1136 (1994).
Hildebrandt, D., and L. T. Biegler, ''Synthesis of Chemical Reactor Networks,'' *AIChE Symp. Ser., Foundation of Computer Aided Process Design*, 52 (1994).
Hildebrandt, D. ,and D. Glasser, ''Attainable Region and Optimal Reactor Structures,'' *Chem. Eng. Sci.*, **45**, 2161 (1990).
Hildebrandt, D., D. Glasser, and C. M. Crowe, ''Geometry of the Attainable Region Generated by Reaction and Mixing. With and Without Constraints,'' *Ind. Eng. Chem. Res.*, **29**, 49 (1990).
Hopley, F., D. Glasser, and D. Hildebrandt, ''Optimal Reactor Structures for Exothermic Reversible Reactions with Complex Kinetics,'' *Chem. Eng. Sci.*, **51**, 2399 (1996).
Horn, F., ''Attainable and Non-Attainable Regions in Chemical Reaction Technique,'' *Proc. Eur. Symp. on Chemical Reaction Engineering*, Pergamon Press, London (1964).
Kokossis, A. C., and C. A. Floudas, ''Optimization of Complex Reactor Networks: I. Isothermal Operation,'' *Chem. Eng. Sci.*, **45**, 595 (1990).
Kokossis, A. C. and C. A. Floudas, ''Optimization of Complex Reactor Networks: II. Nonisothermal Operation,'' *Chem. Eng. Sci.*, **49**, 1037 (1994a).
Kokossis, A. C., and C. A. Floudas, ''Stability in Optimal Design: Synthesis of Complex Reactor Networks,'' *AIChE J.*, **40**, 849 (1994b).
Lakshmanan, A., and L. T. Biegler, ''Synthesis of Optimal Chemical Reactor Networks,'' *Ind. Eng. Chem. Res.*, **35**, 1344 (1966).
Lee, K. Y., and R. Aris, ''Control of a Cold Shot Adiabatic Bed Reactor with a Decaying Catalyst,'' *Ind. Eng. Chem. Proc. Des. Dev.*, 306 (1963).
Marcoulaki, E., and A. C. Kokossis, ''Scoping and Screening of Complex Reaction Networks,'' *AIChE J.*, **45**, 1977 (1999).
Mehta, V. L., and A. C. Kokossis, ''Development of Novel Multi-Phase Reactors Using a Systematic Design Framework,'' *Comput. Chem. Eng.*, **21**, S325 (1997).
Mehta, V. L., and A. C. Kokossis, ''New Generation Tools for Multiphase Reaction Systems: A Validated Systematic Methodology for Novelty and Design Automation,'' *Comput. Chem. Eng.*, **22**, S119 (1998).
Nicole, W., D. Hildebrandt, and D. Glasser, ''Process Synthesis for Reaction Systems with Cooling via Finding the Attainable Region,'' *Comp. Chem. Eng.*, **21** (1997).
Schweiger, C. and C. A. Floudas, ''Optimization Framework for the Synthesis of Chemical Reactor Networks,'' *Ind. Eng. Chem. Res.*, **38**, 744 (1999).

*Manuscript received Dec. 29, 1998, and revision received Apr. 10, 2000.*